$h \to gg$ and $h \to \gamma\gamma$ with anomalous couplings at next-to-leading order in QCD

Gerhard Buchalla,* Marius Höfer,† and Christoph Müller-Salditt‡

Ludwig-Maximilians-Universität München, Fakultät für Physik, Arnold Sommerfeld Center for Theoretical Physics, D-80333 München, Germany

(Received 12 January 2023; accepted 29 March 2023; published 24 April 2023)

We generalize the next-to-leading order (NLO) QCD calculations for the decay rates of $h \to gg$ and $h \to \gamma\gamma$ to the case of anomalous couplings of the Higgs boson. We demonstrate how this computation can be done in a consistent way within the framework of an electroweak chiral Lagrangian, based on a systematic power counting. It turns out that no additional coupling parameters arise at NLO in QCD beyond those already present at leading order. The impact of QCD is large for $h \to gg$ and the uncertainties from QCD are significantly reduced at NLO. $h \to \gamma\gamma$ is only mildly affected by QCD; here the NLO treatment practically eliminates the uncertainties. Consequently, our results will allow for an improved determination of anomalous Higgs couplings from these processes. The relation of our framework to a treatment in Standard Model effective field theory is also discussed.

DOI: 10.1103/PhysRevD.107.076021

I. INTRODUCTION

The discovery of the Higgs boson a decade ago has opened the door for novel tests of the mechanism behind electroweak symmetry breaking. A promising strategy consists in precisely measuring Higgs-boson couplings, which might deviate from their Standard Model (SM) expectation and reveal the presence of new dynamics. Such anomalous couplings are consistently described in the framework of an effective field theory (EFT). A well-motivated and useful tool for this purpose is provided by the electroweak chiral Lagrangian including a light Higgs boson (EWChL, sometimes also referred to as HEFT); see [1,2] and references therein. This nonlinear version of the electroweak EFT has the practical advantage of encoding the anomalous Higgs couplings as the dominant new-physics effects [2]. This allows us to focus on the Higgs-boson properties as our main target, and avoids a proliferation of parameters.

For a reliable determination of Higgs couplings, QCD corrections have to be taken into account in the calculation of Higgs-boson processes. Already in the SM, QCD effects do, in general, have a large numerical impact on the observables [3–8]. Higher-order QCD effects can be combined, in a systematic way, with the anomalous Higgs couplings described by the EWChL [9]. An analysis of this type has been performed in [10] for the case of Higgs-pair production in gluon fusion. In the present paper, we generalize the calculation of the decay rates for $h \to \gamma\gamma$ and $h \to gg$ at next-to-leading order (NLO) in QCD to include new-physics effects in the form of anomalous couplings. We demonstrate how this can be achieved in a consistent manner within the framework of the EWChL.

This paper is organized as follows. In Sec. II we summarize the main properties of the EWChL as an EFT for Higgs processes and define kinematic variables for later use. Section III is devoted to the discussion of $h \to \gamma\gamma$, where the NLO-QCD effects are relatively simple and of moderate size. To set the stage for the EFT treatment of $h \to gg$, we review the results for this process at leading order (LO) in QCD in Sec. IV. Section V describes our main results, the computation of $h \to gg$ in the presence of anomalous couplings and with QCD corrections at NLO. Phenomenological implications of the NLO results for $h \to gg$ are presented in Sec. VI. In Sec. VII we discuss how $h \to \gamma\gamma$ and $h \to gg$ could be treated in Standard Model effective field theory (SMEFT), as an alternative to the EWChL framework we primarily employ. We conclude in Sec. VIII. Some further details and examples are collected in the Appendixes. Appendix A defines the subtraction of IR divergences in the NLO rate of $h \to gg$. Appendix B explains in detail the dependence of the $h \to gg$ rate at NLO on the anomalous couplings in

*gerhard.buchalla@lmu.de
†m.hoefer@physik.uni-muenchen.de
‡christoph.mueller1@physik.uni-muenchen.de

the region where the rate becomes small due to cancellations. In Appendix C we give the LO and NLO correlation matrices for the parametric uncertainties of the $h \to gg$ decay rate. Finally, Appendix D illustrates the matching of the local $h\gamma\gamma$ and hgg couplings in the EFT to a UV theory in a few toy model scenarios, with a particular view on the role of QCD corrections in this context.

II. EFT LAGRANGIAN AND KINEMATIC VARIABLES

The EWChL at lowest order is given by [11,12]

$$\begin{aligned}\mathcal{L}_2 = &-\frac{1}{4}G^a_{\mu\nu}G^{a\mu\nu} - \frac{1}{2}\langle W_{\mu\nu}W^{\mu\nu}\rangle \\ &-\frac{1}{4}B_{\mu\nu}B^{\mu\nu} + \frac{v^2}{4}\langle D_\mu U^\dagger D^\mu U\rangle F(\eta) \\ &+\frac{v^2}{2}\partial_\mu\eta\partial^\mu\eta - V(\eta) + \bar\psi i\not{D}\psi - \bar\psi m(\eta,U)\psi, \end{aligned} \tag{2.1}$$

where $\eta \equiv h/v$ with h the Higgs singlet and $v = 246$ GeV the electroweak scale. $G^a_{\mu\nu}$, $W^\alpha_{\mu\nu}$ and $B_{\mu\nu}$ are the gauge field strengths of $SU(3)_C$, $SU(2)_L$ and $U(1)_Y$, respectively. Here $\langle\cdots\rangle$ denotes the trace over $SU(2)_L$ indices.

The electroweak Goldstone bosons φ^α are collected in $U = \exp(2i\varphi/v)$, where $\varphi = \varphi^\alpha t^\alpha$ and t^α denote the generators of $SU(2)_L$, normalized as $\langle t^\alpha t^\beta\rangle = \delta^{\alpha\beta}/2$. The covariant derivative of the Goldstone field reads

$$D_\mu U = \partial_\mu U + igW_\mu U - ig' B_\mu U t^3 \tag{2.2}$$

with $SU(2)_L$ and $U(1)_Y$ gauge couplings g and g', respectively. All SM fermions are collectively written as $\psi = (u_i, d_i, \nu_i, e_i)^T$, where u_i, d_i, ν_i, and e_i are Dirac spinors and i is the generation index. The Yukawa term is then given by the last term in (2.1) with

$$m(\eta,U) \equiv U\mathcal{M}(\eta)P_R + \mathcal{M}^\dagger(\eta)U^\dagger P_L, \tag{2.3}$$

where $\mathcal{M}$ is the block-diagonal mass matrix

$$\mathcal{M} = \mathrm{diag}(\mathcal{M}_u, \mathcal{M}_d, \mathcal{M}_\nu, \mathcal{M}_e) \tag{2.4}$$

acting on ψ. In general, the entries $\mathcal{M}_f \equiv \mathcal{M}_f(\eta)$ with $f = \{u, d, \nu, e\}$ are h-dependent matrices in generation space.

The Higgs-dependent functions are expanded as

$$\begin{aligned} F(\eta) &= 1 + \sum_{n=1}^{\infty} F_n \eta^n, \qquad V(\eta) = v^4 \sum_{n=2}^{\infty} V_n \eta^n, \\ \mathcal{M}_f(\eta) &= \sum_{n=0}^{\infty} \mathcal{M}_{f,n}\eta^n \end{aligned} \tag{2.5}$$

so that the fermion masses are given by $m_f = \mathcal{M}_{f,0}$. In comparison with the SM, the Lagrangian in (2.1) introduces anomalous couplings in the Higgs sector, out of which only a restricted subset is usually relevant for a given application. For instance, we can introduce $c_f = \mathcal{M}_{f,1}/m_f$, which parametrizes potential deviations from the $h\bar f f$ vertex in the SM. Similarly, assuming custodial symmetry, an anomalous coupling $c_V \equiv F_1/2$ for the hW^+W^- and hZZ vertices can be defined [2].

Going beyond lowest order in the loop expansion, new terms have to be added to $\mathcal{L}_2$. The terms entering at one-loop order in the EWChL are denoted by $\mathcal{L}_4$ and can be found in [11,13,14]. This introduces further anomalous couplings and also provides the necessary counterterms for one-loop diagrams from (2.1). For our purpose, it is sufficient to focus only on new local interactions between the Higgs boson and the massless gauge bosons with couplings $c_{\gamma\gamma h}$ and c_{ggh}, respectively; see Fig. 1.

To summarize, the CP-even terms from the effective Lagrangian $\mathcal{L}_{\rm eff} \equiv \mathcal{L}_2 + \mathcal{L}_4$ with anomalous couplings relevant for the Higgs decays to two photons or gluons read

$$\begin{aligned}\mathcal{L}_{\rm eff} \supset\ & 2c_V\frac{h}{v}\left(m_W^2 W_\mu^+ W^{-\mu} + \frac{1}{2}m_Z^2 Z_\mu Z^\mu\right) - \sum_f m_f c_f \frac{h}{v}\bar f f \\ &+ \frac{\alpha}{8\pi}c_{\gamma\gamma h}\frac{h}{v}F_{\mu\nu}F^{\mu\nu} + \frac{\alpha_s}{8\pi}c_{ggh}\frac{h}{v}G^a_{\mu\nu}G^{a\mu\nu}, \end{aligned} \tag{2.6}$$

where $\alpha = e^2/4\pi$ and $\alpha_s = g_s^2/4\pi$ are the electromagnetic and strong fine structure constants, respectively. As stated above, the anomalous couplings c_f and c_V arise from $\mathcal{L}_2$ and are leading-order effects in the EFT counting, whereas the local Higgs-gluon and Higgs-photon couplings $c_{\gamma\gamma h}$ and c_{ggh} are introduced by $\mathcal{L}_4$ and thus enter at NLO (one-loop) order. In the SM we have $c_f = c_V = 1$ and $c_{\gamma\gamma h} = c_{ggh} = 0$. However, all couplings may have arbitrary values of $\mathcal{O}(1)$ in general. In the following, we will neglect the couplings of

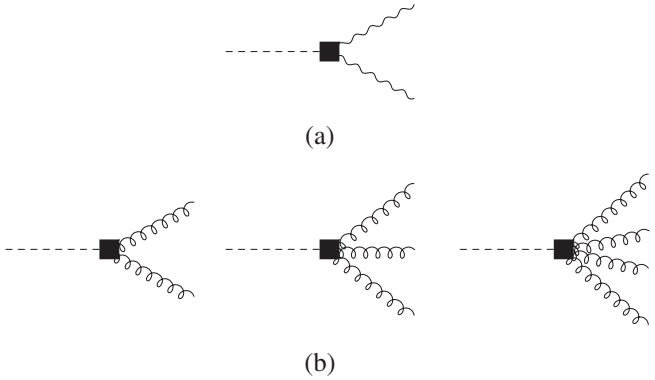

FIG. 1. New local vertices of the Higgs to photons (a) and gluons (b). The Higgs-photon coupling (a) is generated by the second to last term of (2.6). It is proportional to $c_{\gamma\gamma h}$ and of order e^2. The three Higgs-gluon couplings (b) are generated by the last term of (2.6). They are all proportional to c_{ggh} and are of order g_s^2, g_s^3, and g_s^4, respectively.

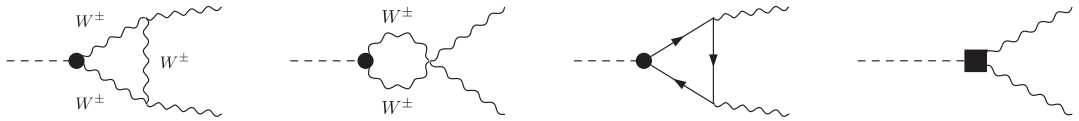

FIG. 2. Diagrams contributing to the LO, i.e. $\mathcal{O}(g_s^0)$, amplitudes A_W, A_ℓ, $A_q^{(0)}$, and A_h of the decay $h \to \gamma\gamma$. Here and in the following, black dots and black squares indicate vertices from $\mathcal{L}_2$ and $\mathcal{L}_4$, respectively. The fermion can be both a quark or charged lepton, as long as it is massive. Clockwise and counterclockwise fermion flow is implicitly understood.

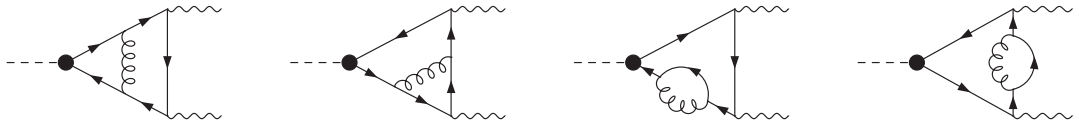

FIG. 3. Diagrams contributing to the virtual corrections $A_q^{(1)}$ to the decay $h \to \gamma\gamma$ at $\mathcal{O}(g_s^2)$. Only the quark-loop diagrams receive QCD corrections at this level.

the Higgs to the first two lepton generations as well as to up-quarks, down-quarks and strange-quarks due to their small masses.

We conclude this section by defining some kinematical variables, which are useful for presenting the rates of $h \to \gamma\gamma$ and $h \to gg$, namely

$$\tau_i = \frac{m_h^2}{4m_i^2} + i0^+ \tag{2.7}$$

and

$$x_i = \frac{\sqrt{1-\tau_i^{-1}}-1}{\sqrt{1-\tau_i^{-1}}+1} + i0^+, \tag{2.8}$$

where, for the purpose of analytic continuation, we always assume a small positive imaginary part. In the SM, the leading order decay of Higgs to both photons and gluons is loop induced; m_i in (2.7) usually denotes the mass of the particle running in the loop. We can then distinguish between configurations above and below the particle pair production threshold:

$$\text{below threshold: } 0 < \tau_i < 1 \qquad x_i = e^{i\theta_i} \quad (0 < \theta_i < \pi) \tag{2.9}$$

$$\text{above threshold: } 1 \le \tau_i < \infty \qquad -1 \le x_i < 0. \tag{2.10}$$

III. HIGGS DECAY TO PHOTONS

The decay rate of a Higgs into a pair of photons is given by

$$\Gamma_{h\to\gamma\gamma} = \frac{\alpha^2}{256\pi^3}\frac{m_h^3}{v^2}|A_{h\to\gamma\gamma}|^2, \tag{3.1}$$

where up to $\mathcal{O}(\alpha_s)$

$$A_{h\to\gamma\gamma} = c_{\gamma\gamma h}A_h + c_V A_W(\tau_W) + \sum_\ell c_\ell A_\ell(\tau_\ell) + N_c\sum_q c_q Q_q^2\left(A_q^{(0)}(\tau_q) + \frac{\alpha_s}{4\pi}A_q^{(1)}(\tau_q)\right). \tag{3.2}$$

The different subamplitudes A_i describe the coupling of the Higgs to photons either directly (A_h) or through a $W^\pm$ loop (A_W), charged-lepton loop (A_ℓ) or a quark loop ($A_q^{(0,1)}$); see Fig. 2. Only the latter receives QCD corrections at this perturbative order in α_s; see Fig. 3. The loop functions A_q and their coefficients c_q are separately renormalization-scale independent. We have chosen the normalization of $A_{h\to\gamma\gamma}$ such that[1]

$$A_h = 1. \tag{3.3}$$

The coefficient $c_{\gamma\gamma h}$ implicitly contains $\mathcal{O}(\alpha_s)$ corrections, as will be further discussed in Appendix D. The one-loop functions in Eq. (3.2) are well known from the SM. They read [15,16]

$$A_W(\tau) = -\frac{2\tau^2+3\tau+3(2\tau-1)f(\tau)}{\tau^2} = -\frac{2(x^2-8x+1)}{(x-1)^2} - \frac{6x(x^2+1)}{(x-1)^4}\ln^2 x, \tag{3.4}$$

$$A_\ell(\tau) = A_q^{(0)}(\tau) = \frac{2(\tau+(\tau-1)f(\tau))}{\tau^2} = -\frac{8x}{(x-1)^2} + \frac{2x(x+1)^2}{(x-1)^4}\ln^2 x, \tag{3.5}$$

[1]Note that the local $h\gamma\gamma$ coupling $c_{\gamma\gamma h}$ used here is related to the coupling $c_{\gamma\gamma}$ defined in [9] through $c_{\gamma\gamma h} \equiv 2c_{\gamma\gamma}$.

TABLE I. Loop functions contributing to the decay $h \to \gamma\gamma$ and their correspondence in the literature. [4,24] set $N_c = 3$, in [25] the number of colors is left arbitrary. $A_q^{(1),a}$ corresponds to Eq. (10) in [23], which, however, contains typos. See footnote 3 of [24].

Reference	A_W	$A_\ell = A_q^{(0)}$	$A_q^{(1),a}$	$-6C_F\tau\frac{\partial A_q^{(0)}}{\partial\tau}$
[4,24]	A_W^H	$\frac{4}{3}F_0^H$	$4C_F F_0^H C_1^H$	$4C_F F_0^H C_2^H = 2C_F F_0^H B_2^H$
[25]	$-\mathcal{F}_1^{(1\ell)}$	$-\mathcal{F}_{1/2}^{(1\ell)}$	$-4C_F(\mathcal{F}_{1/2}^{(2\ell,a)} + \frac{4}{3}\mathcal{F}_{1/2}^{(2\ell,b)})$	$4C_F\mathcal{F}_{1/2}^{(2\ell,b)}$

with x defined in (2.8) and

$$f(\tau) = \arcsin^2\sqrt{\tau} = -\frac{1}{4}\ln^2 x, \tag{3.6}$$

which is real valued below the pair production threshold, $0 < \tau < 1$, and complex valued otherwise.

The NLO QCD corrections to the quark loop [4,17–25] (Fig. 3) can be decomposed as

$$A_q^{(1)}(\tau) = A_q^{(1),a}(\tau) - 6C_F\tau\frac{\partial A_q^{(0)}(\tau)}{\partial\tau}X(\mu_q^2), \tag{3.7}$$

where the function X depends on the quark mass renormalization scheme. We have

$$X(\mu_q^2) = \begin{cases} 0 & (\text{OS}) \\ \ln(\mu_q^2/m_q^2) + \frac{4}{3} & (\overline{\text{MS}}, \text{scheme of [25]}), \end{cases} \tag{3.8}$$

where μ_q is the scale at which the mass is renormalized in the case of a running mass scheme, which is not necessarily identical to the renormalization scale μ_R of the strong coupling constant α_s. The relation between the quark mass in the on-shell (OS) scheme, m_{OS}, and the $\overline{\text{MS}}$ scheme, $\bar{m}(\mu_q)$, to one loop in QCD is

$$m_{\text{OS}} = \bar{m}(\mu_q)\left(1 + \frac{\alpha_s(\bar{m})}{\pi}\left(\ln\frac{\mu_q^2}{\bar{m}^2} + \frac{4}{3}\right)\right). \tag{3.9}$$

We remark that in [24] the running mass is defined as in Eq. (5) of [4], which is different from the $\overline{\text{MS}}$ mass. This alternative definition corresponds to

$$X(\mu_q^2) = \ln(\mu_q^2/m_q^2) \quad (\text{scheme of [4, 24]}). \tag{3.10}$$

The remainder $A_q^{(1),a}$ of the two-loop function can be found in the literature, see Table I.

Note that the emission of a single gluon off the quark loop ($h \to \gamma\gamma g$) is forbidden by color symmetry. Therefore, there are no real radiation corrections of $\mathcal{O}(g_s)$ relative to the Born amplitude. As a consequence, the virtual QCD corrections are infrared finite, as any singularities would need to cancel against phase-space singularities in the real corrections by virtue of the Kinoshita-Lee-Nauenberg-Theorem (KLN) theorem [26,27]. This enables us to consider an IR-finite expansion in g_s already at the amplitude level, given in (3.2) to $\mathcal{O}(\alpha_s)$. The decay rate in (3.1) is then exact to $\mathcal{O}(\alpha_s)$ (NLO QCD) and contains parts of the $\mathcal{O}(\alpha_s^2)$ [next-to-next-to-leading order (NNLO) QCD] corrections. However, to fully capture NNLO QCD, one would also have to include genuine $\mathcal{O}(\alpha_s^2)$ contributions, that is three-loop diagrams for $h \to \gamma\gamma$, the emission of two gluons from the quark loop (double real corrections), as well as two-loop diagrams for $h \to \gamma\gamma$ containing local hgg vertices. Those contributions are beyond the scope of this work.

We close this section with a brief discussion of the numerical impact of the NLO QCD effects. We checked all formulas by independent calculations, except for the function $A_q^{(1),a}$. The numbers were obtained with two independent codes. As an additional check we compared with the publicly available program eHDECAY [28], which implements the results from [29]. It contains the $h \to \gamma\gamma$ decay rate as presented in (3.1) and (3.2). Testing several different values of the effective couplings c_i in (3.2), we found agreement within the uncertainties of the different implementations for all cases.

Using input parameters from [30], see also Table II, we calculate the central values for the various loop contributions to the $h \to \gamma\gamma$ amplitude. They are listed in Table III. These numbers quantify the relative importance of the subamplitudes. W and top-quark contributions are dominant, τ, b and c loops only matter when very high precision is required. The lighter fermions are negligible. Note that here, in contrast to the SM case, the relative weighting of

TABLE II. Input parameters for the calculation of the coefficients A_i, corresponding to the 2022 PDG [30] values. The Higgs vacuum expectation value is derived through its relation to the Fermi constant $G_F = (\sqrt{2}v^2)^{-1}$.

Parameter	Value
m_h	125.25(17) GeV
m_t (OS mass)	172.69(30) GeV
m_b (OS mass)	4.78(6) GeV
m_c (OS mass)	1.67(7) GeV
m_τ	1.77686(12) GeV
m_W	80.377(12) GeV
m_Z	91.1876(21) GeV
$\alpha_s(m_Z)$	0.1179(9)
G_F	$1.1663788(6) \times 10^{-5}$ GeV^{-2}

TABLE III. Numerical values for the $h \to \gamma\gamma$ amplitude functions A_i. The quark contributions A_q include the NLO QCD corrections, where the quark mass is defined as the pole mass.

A_W	A_τ	A_μ	$\frac{4}{3}A_t$	$\frac{1}{3}A_b$	$\frac{4}{3}A_c$
-8.33	$-0.024 + 0.022i$	$(-3+i)10^{-4}$	1.78	$-0.027 + 0.023i$	$-0.022 + 0.009i$

the subamplitudes is affected by the anomalous couplings in (3.2).

The loops with light fermions have imaginary parts. Their contribution to the rate is completely negligible: Assuming SM couplings, $|A_{h\to\gamma\gamma}|/|\mathrm{Re}A_{h\to\gamma\gamma}|$ deviates from unity by less than 10^{-4}.

We illustrate the impact of QCD corrections on A_t, the dominant contribution from quark loops, using the scheme in (3.10). For $\mu_t = m_t$ this corresponds to the pole mass. Using central parameter values and showing the uncertainty from scale dependence ($m_t/2 < \mu_t < 2m_t$), we find at LO and NLO, respectively,

$$A_t^{\mathrm{LO}} = 1.3766^{+0.0046}_{-0.0045}, \tag{3.11}$$

$$A_t^{\mathrm{NLO}} = 1.3351^{+0.0000}_{-0.0008}. \tag{3.12}$$

The central value is reduced by about three percent at NLO. At the same time, the small LO uncertainty of three permille is reduced by another order of magnitude at NLO and thus essentially eliminated.

A convenient analytical expression for the top-quark function at NLO can be obtained from an expansion in the variable τ. To linear order in τ it reads

$$A_t(\tau) = \frac{4}{3} + \frac{14}{45}\tau + \frac{\alpha_s}{\pi}\left(-\frac{4}{3} + \frac{488}{405}\tau - \frac{28}{45}\tau X(\mu_q^2)\right), \tag{3.13}$$

which is accurate at the permille level.

For SM couplings we find with our central parameter set

$$\Gamma_{h\to\gamma\gamma} = 9.54\ \mathrm{keV}, \tag{3.14}$$

including the NLO QCD corrections (the LO value is 9.41 keV). The error from scale dependence in the t, b and c amplitudes is safely below a permille.

Displaying the dependence of the rate on the anomalous couplings we may write

$$\begin{aligned}\Gamma_{h\to\gamma\gamma}/\mathrm{keV} = {} & 15.098c_W^2 - 6.451c_t c_W - 3.624c_{\gamma\gamma h}c_W + 0.774c_{\gamma\gamma h}c_t + 0.689c_t^2 + 0.217c_{\gamma\gamma h}^2 - 0.012c_b c_{\gamma\gamma h} - 0.009c_c c_{\gamma\gamma h} \\ & - 0.021c_b c_t - 0.017c_c c_t - 0.010c_{\gamma\gamma h}c_\tau - 0.018c_t c_\tau + 0.097c_b c_W + 0.079c_c c_W + 0.085c_\tau c_W.\end{aligned} \tag{3.15}$$

Here we have dropped terms with coefficients of less than 0.001. Again, the NLO QCD uncertainties are negligible.

IV. $h \to gg$ AT LO IN QCD

At LO the decay rate of a Higgs into two gluons is given by

$$\Gamma_{h\to gg}^{\mathrm{LO}} = \frac{\alpha_s^2}{256\pi^3}\frac{m_h^3}{v^2}(N_c^2 - 1)|A_{h\to gg}^{(0)}|^2, \tag{4.1}$$

where

$$A_{h\to gg}^{(0)} = c_{ggh}A_h^{(0)} + \frac{1}{2}\sum_q c_q A_q^{(0)}(\tau_q). \tag{4.2}$$

The first term is the local Higgs-gluon interaction [Fig. 4 (right)]. As for the $h \to \gamma\gamma$ amplitude, we have chosen the normalization of $A_{h\to gg}^{(0)}$ such that

$$A_h^{(0)} = 1. \tag{4.3}$$

The second term of (4.2) accounts for the SM-like contribution from heavy-quark loops [Fig. 4 (left)]. Note that compared to (3.2), there is a different overall factor of the triangle contribution $A_q^{(0)}(\tau_q)$, stemming from the different color structures of the quark-gluon and quark-photon vertices.[2] $A_q^{(0)}(\tau_q)$ is the same function which we already encountered in $h \to \gamma\gamma$; see Table I. Compact tree-level helicity amplitudes for the decay of a scalar particle like the Higgs into an arbitrary number of fermions and gluons via the interaction term $hG^a_{\mu\nu}G^{a\mu\nu}$ can be found in [31,32].

In order to examine the effect of variations of the effective couplings c_{ggh} and c_q, the decay rate can be expressed as a polynomial bilinear in the couplings,

$$\begin{aligned}\Gamma_{h\to gg}^{\mathrm{LO}} = {} & A_{gg}^{\mathrm{LO}}c_{ggh}^2 + A_{tt}^{\mathrm{LO}}c_t^2 + A_{bb}^{\mathrm{LO}}c_b^2 + A_{tg}^{\mathrm{LO}}c_{ggh}c_t \\ & + A_{bg}^{\mathrm{LO}}c_{ggh}c_b + A_{bt}^{\mathrm{LO}}c_t c_b,\end{aligned} \tag{4.4}$$

[2]We have T^a_{ij} for the quark-gluon and $Q_q\delta_{ij}$ for the quark-photon vertex with T^a the $SU(N_c)$ generators in the fundamental representation ($i, j = 1, \ldots, N_c$) and normalization $\mathrm{Tr}[T^a T^b] = \frac{1}{2}\delta^{ab}$.

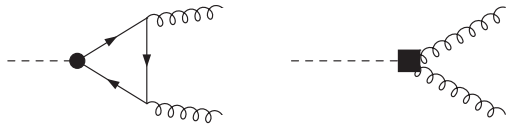

FIG. 4. Diagrams contributing to the decay $h \to gg$ at LO, both in the chiral counting (one-loop order) and in the QCD coupling (order g_s^2).

where we considered only third generation quarks, i.e. $q = b,\ t$. The contributions from the other quarks are negligible due to their small mass and hence their suppressed coupling to the Higgs. Unlike in the $h \to \gamma\gamma$ decay there is no enhancement of the c-quark with respect to the b-quark contribution by electromagnetic charge factors.

V. $h \to gg$ AT NLO IN QCD

At NLO in QCD we have to consider both virtual (V) and real radiation (R) corrections. The former consist of all $\mathcal{O}(g_s^4)$, two-loop order $h \to gg$ diagrams, the latter comprise all $\mathcal{O}(g_s^3)$ one-loop order diagrams with one extra massless colored particle in the final state, i.e. $h \to ggg$ and $h \to gq\bar{q}$, where q ($\bar{q}$) is a massless quark (antiquark).

The NLO decay rate can be written as

$$\Gamma^{\mathrm{NLO}}_{h\to gg} = \Gamma^{\mathrm{LO}}_{h\to gg} + \Gamma^{V}_{h\to gg} + \Gamma^{R}_{h\to gg}. \tag{5.1}$$

Both the virtual and the real radiation contribution are in fact infrared (IR) divergent: the former due to explicit poles in $\epsilon = (4-D)/2$ from the dimensionally regulated loop integrals (D is the number of space-time dimensions), the latter due to phase-space configurations with soft or collinear partons for which the matrix elements are singular. The singularities cancel in the sum of both contributions and we obtain a finite, physically meaningful result. In practice a suitable IR scheme has to be chosen to deal with the cancellation of the singularities. We adopt the antenna subtraction formalism [33–35].

Similarly to the LO rate in (4.4), we write the NLO decay rate as a polynomial in the effective couplings,

$$\Gamma^{\mathrm{NLO}}_{h\to gg} = A^{\mathrm{NLO}}_{gg} c^2_{ggh} + A^{\mathrm{NLO}}_{tt} c_t^2 + A^{\mathrm{NLO}}_{bb} c_b^2 + A^{\mathrm{NLO}}_{tg} c_{ggh} c_t + A^{\mathrm{NLO}}_{bg} c_{ggh} c_b + A^{\mathrm{NLO}}_{bt} c_t c_b. \tag{5.2}$$

A. Virtual corrections

There are three distinct classes of diagrams contributing to the virtual corrections, see Figs. 5 and 6:

(1) genuine two-loop diagrams with vertices from $\mathcal{L}_2$ only;
(2) one-loop diagrams with a single one-loop order effective vertex of chiral dimension 4, i.e. from $\mathcal{L}_4$;
(3) one tree-level diagram with an effective vertex of chiral dimension six coming from $\mathcal{L}_6$.

Diagrams of the first class are shown in Fig. 5(a). Up to the rescaling by the effective couplings c_q they correspond to the diagrams needed to calculate the two-loop amplitude in the ordinary SM with full mass dependence. The second class of diagrams [Fig. 5(b)] associated with c_{ggh} has no correspondence in the SM. While $\mathcal{L}_4$ also provides $hggg$

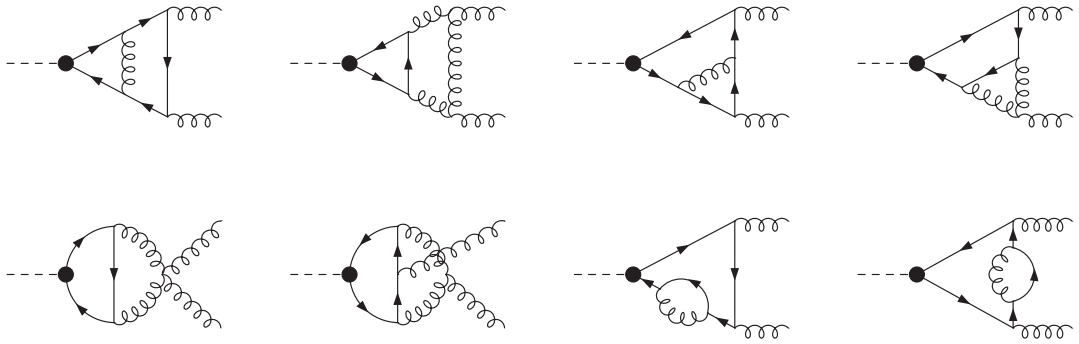

(a)

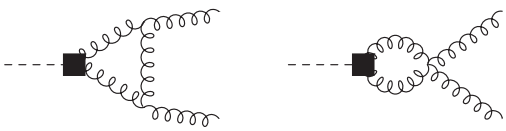

(b)

FIG. 5. Diagrams contributing to the virtual corrections to the decay $h \to gg$ at $\mathcal{O}(g_s^4)$. (a) Genuine two-loop diagrams with vertices from $\mathcal{L}_2$ only. (b) One-loop diagrams with one effective vertex from $\mathcal{L}_4$.

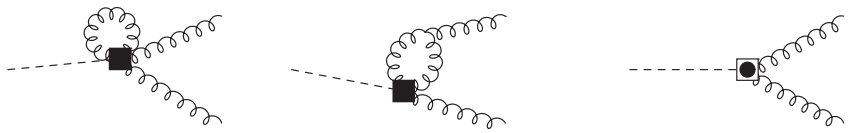

(a) (b)

FIG. 6. Diagrams of two-loop order not contributing to the virtual corrections of $\mathcal{O}(g_s^4)$. While being of $\mathcal{O}(g_s^4)$, the scaleless diagrams (a) vanish by virtue of dimensional regularization. Diagram (b) contains an effective hgg vertex coming from the NNLO chiral Lagrangian $\mathcal{L}_6$. It gives no additional contribution to the considered order as further discussed in the text.

and $hgggg$ vertices of the right order in g_s, the relevant one-loop diagrams [Fig. 6(a)] vanish when evaluated in dimensional regularization. Higgs plus multiparton one-loop amplitudes with local Higgs-gluon interactions have been calculated in [36]. At last there is the single tree-level diagram with an effective vertex of chiral dimension six [Fig. 6(b)]. Such a diagram could in principle contribute at the order under consideration, that is two-loop order in the EWChL and at $\mathcal{O}(g_s^4)$. However, from gauge invariance any local hgg vertex can be expressed by an operator $hG^a_{\mu\nu}G^{a\mu\nu}$, which is identical to the corresponding term already included in $\mathcal{L}_4$. In fact, a $d_\chi = 6$ operator such as

$$\mathcal{O}_{6,hgg} = g_s^2 D_\rho G^a_{\mu\nu} G^{a\mu\nu} \partial^\rho h, \tag{5.3}$$

or similar terms, can be eliminated using integration by parts and equations of motion (eom) in favor of the operator $hG^a_{\mu\nu}G^{a\mu\nu}$. For example,

$$\begin{aligned}\mathcal{O}_{6,hgg} &= -\frac{1}{2} g_s^2 G^a_{\mu\nu} G^{a\mu\nu} \partial^2 h \\ &= \frac{1}{2v} g_s^2 G^a_{\mu\nu} G^{a\mu\nu} \left(V' - \frac{v^2}{4} \langle D_\mu U^\dagger D^\mu U \rangle F' + \bar{\psi} m' \psi \right) \\ &= \frac{m_h^2}{2} g_s^2 G^a_{\mu\nu} G^{a\mu\nu} h + \cdots,\end{aligned} \tag{5.4}$$

where we dropped total derivatives and, in the last step, terms with additional fields, which do not contribute at the relevant order. In general, local terms with $d_\chi = 6$ for the hgg vertex therefore correspond to subleading contributions in the coefficient

$$c_{ggh} = c^{(0)}_{ggh} + \mathcal{O}(g_s^2, m_h^2/\Lambda^2), \tag{5.5}$$

with the leading term $c^{(0)}_{ggh} = \mathcal{O}(1)$. The g_s^2 corrections are part of the NLO QCD effects, as will be further discussed in Appendix D. The terms $\sim m_h^2/\Lambda^2$ are formally negligible at the considered order. They do not scale as g_s^4 and are not part of the NLO QCD corrections. In practice, all these effects are implicitly contained in the coefficient c_{ggh}.

Other terms at $d_\chi = 6$ contribute only beyond the order we are considering. For instance, the operator

$$\mathcal{O}_{6,hgq} = g_s^2 D^\mu G^a_{\mu\nu} G^{a\nu\lambda} \partial_\lambda h = g_s^3 \bar{q} \gamma_\nu T^a q G^{a\nu\lambda} \partial_\lambda h, \tag{5.6}$$

where we have used the gluon eom in the last step, can interfere with the diagrams in Fig. 7(b). However, this is one loop order higher than the squares of Fig. 7(b) entering at NLO, and can be consistently neglected.

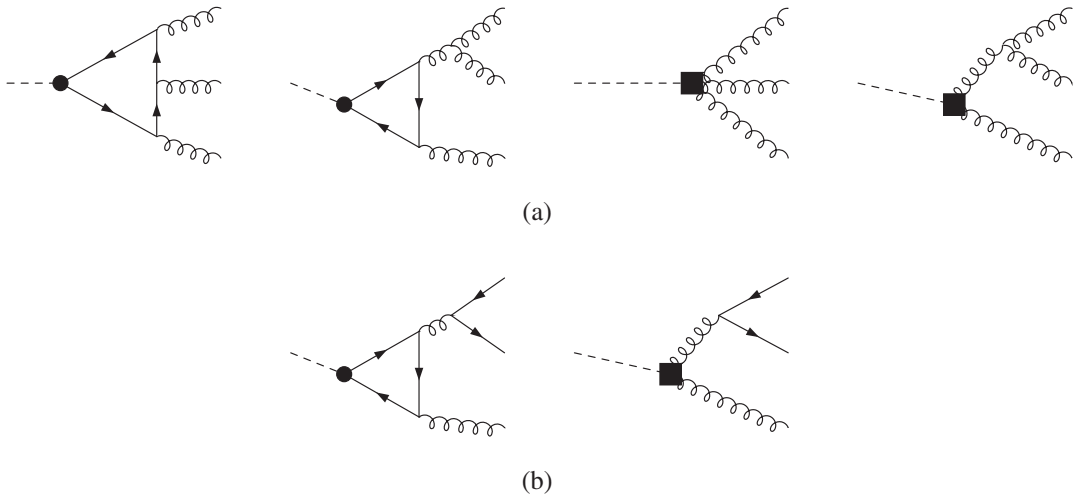

(a) (b)

FIG. 7. Example diagrams contributing to the real emission corrections to the decay $h \to gg$ at $\mathcal{O}(g_s^3)$ at the amplitude level: (a) ggg decay channel; (b) $gq\bar{q}$ decay channel.

TABLE IV. References for the two-loop corrections to the quark-loop contribution to the $h \to gg$ rate and the expressions therein, which correspond to the functions introduced in this paper. [4,24] set $N_c = 3$, [25,38] keep the number of colors arbitrary.

Reference	$A_{q,g}^{(1),a}$	$-6C_F\tau\frac{\partial A_q^{(0)}}{\partial\tau}$
[4,24]	$\frac{8}{9}C_A(F_0^H B_1^H - 2F_0^H C_1^H) + 4C_F F_0^H C_1^H$	$4C_F F_0^H C_2^H = 2C_F F_0^H B_2^H$
[25]	$-4C_A\mathcal{G}_{1/2}^{(2\ell,C_A)} - 4C_F(\mathcal{F}_{1/2}^{(2\ell,a)} + \frac{4}{3}\mathcal{F}_{1/2}^{(2\ell,b)})$	$4C_F\mathcal{F}_{1/2}^{(2\ell,b)}$
[38]	$M_{f,\mathrm{fin}}^{(1)} - 6C_F m_q^2\frac{\partial M_f^{(0)}}{\partial m_q^2}(\frac{4}{3} + \log\frac{m_h^2}{m_q^2})$	$6C_F m_q^2\frac{\partial M_f^{(0)}}{\partial m_q^2}$

The contribution of the virtual corrections to the decay rate is given by

$$\Gamma_{h\to gg}^V = \frac{\alpha_s^3}{512\pi^4}\frac{m_h^3}{v^2}(N_c^2-1)\mathrm{Re}\{A_{h\to gg}^{(0)\dagger}A_{h\to gg}^{(1)}\}, \tag{5.7}$$

where we explicitly pulled out the coupling factor $\alpha_s/4\pi$ from the NLO part of the amplitude as in (3.2) with

$$A_{h\to gg}^{(1)} = N_c I(\epsilon)A_{h\to gg}^{(0)}(\epsilon) + \frac{1}{2}\sum_q c_q A_{q,g,\mathrm{fin}}^{(1)}(\tau_q) + \mathcal{O}(\epsilon). \tag{5.8}$$

The renormalization of the amplitude is carried out in the $\overline{\mathrm{MS}}$ scheme, apart from the quark mass, for which we also considered the OS scheme and the scheme from [4,24]. The IR finite part of the amplitude can then be decomposed as

$$A_{q,g,\mathrm{fin}}^{(1)}(\tau) = A_{q,g}^{(1),a}(\tau) - 6C_F\tau\frac{\partial A_q^{(0)}(\tau)}{\partial\tau}X(\mu_q^2), \tag{5.9}$$

where $X(\mu_q^2)$ is defined above, see Eqs. (3.8) and (3.10), and the expression $A_{q,g}^{(1),a}(\tau_q)$ can be found in the literature, see Table IV. The IR singular behavior is contained in[3]

$$I(\epsilon) = -\frac{2}{\epsilon^2} - \frac{1}{\epsilon}\left(\frac{\beta_0}{N_c} + 2L\right) - L^2 + \frac{\pi^2}{6}, \tag{5.10}$$

where

$$\beta_0 = \frac{11}{3}N_c - \frac{2}{3}N_F \tag{5.11}$$

is the first term of the QCD β function and $L = \log\mu_R^2/m_h^2 + i\pi$, with μ_R the renormalization scale. $I(\epsilon)$ multiplies the LO amplitude, for which we now also have to consider terms up to $\mathcal{O}(\epsilon^2)$,

$$A_{h\to gg}^{(0)}(\epsilon) = c_{ggh}S_\epsilon^{-1}A_h^{(0)} + \frac{1}{2}\sum_q c_q\left(\frac{m_q^2}{\mu_R^2}\right)^{-\epsilon}A_q^{(0)}(\tau_q,\epsilon) \tag{5.12}$$

with $S_\epsilon = (4\pi)^\epsilon e^{-\gamma\epsilon}$ and $\gamma = 0.57721\ldots$ is the Euler-Mascheroni constant. $A_q^{(0)}(\tau_q,\epsilon)$ corresponds to $M_{\mathrm{f}}^{(0)} = -\bar{\mathcal{M}}_{\mathrm{f}}^{(0)}$ from [38]. Its zeroth order term is just the LO expression $A_q^{(0)}(\tau_q)$. We work in the $N_F = 5$ scheme, i.e. all quarks besides the top are considered as massless, except for the bottom quark in the loop contribution to $h \to gg$.

B. Real radiation corrections

Moving on to the real corrections, we have to consider diagrams where in comparison to the Born level expression, an additional gluon is radiated into the final state [Fig. 7(a)]. This includes a contribution featuring an effective $hggg$ vertex. Originating from the same term in $\mathcal{L}_4$ as the hgg vertex, it also comes with the coupling c_{ggh}.

Besides the $h \to ggg$ channel, we have to include the possibility of a gluon splitting into a massless quark-antiquark pair, i.e. the channel $h \to g(g \to q\bar{q})$ [Fig. 7(b)]. This is because in the collinear configuration, the $q\bar{q}$ pair is indistinguishable from a gluon. As mentioned above, we consider $N_F = 5$ massless quark flavors. Note that since the coupling of the Higgs to quarks is directly proportional to the quark mass, there are no diagrams contributing to the $h \to gq\bar{q}$ channel where the Higgs couples directly to the light massless quarks and the final state gluon is radiated off the quark line. The real emission contribution to the decay rate is then simply the sum of both channels,

$$\Gamma_{h\to gg}^R = \Gamma_{h\to gg}^{R,ggg} + N_F\Gamma_{h\to gg}^{R,gq\bar{q}}. \tag{5.13}$$

[3]This object is closely related to Catani's one-loop insertion operator $\boldsymbol{I}_{ij}^{(1)}(\epsilon)$ [37] via

$$I(\epsilon) = \frac{2}{N_c}\boldsymbol{I}_{gg}^{(1)}(\epsilon) + \frac{\beta_0}{N_c}L + \mathcal{O}(\epsilon).$$

1. $h \to ggg$ channel

The contribution of the ggg channel to the NLO decay rate is given by

$$\Gamma^{R,ggg}_{h\to gg} = \frac{\alpha_s^3}{24\pi m_h v^2} N_c(N_c^2-1) \times \int \mathrm{d}\Phi_3(p_1,p_2,p_3) \sum_\lambda \mathcal{H}^\lambda(s_{12},s_{23},s_{13}) \times \left|A^{(0)\lambda}_{h\to ggg}(s_{12},s_{23},s_{13})\right|^2, \tag{5.14}$$

where $s_{ij} = (p_i + p_j)^2$ with p_i and p_j denoting either two of the outgoing gluon momenta (we have $s_{12}+s_{23}+s_{13} = m_h^2$). Adjusted to the case at hand (decay of a scalar particle), the three-body phase space reads

$$\mathrm{d}\Phi_3(p_1,p_2,p_3) = \frac{(2\pi)^{2\epsilon-3}}{2^{4-2\epsilon}\Gamma(2-2\epsilon)} \times (m_h^2)^{\epsilon-1}(s_{12}s_{23}(m_h^2-s_{12}-s_{23}))^{-\epsilon}\mathrm{d}s_{12}\mathrm{d}s_{23}. \tag{5.15}$$

The form of the amplitude depends on the concrete helicity configurations λ of the three gluons, so the helicity summation has to be left explicit. We factored out the object $\mathcal{H}^\lambda$ which captures the helicity dependence of the tree-level contribution, so that

$$A^{(0)\lambda}_{h\to ggg}(s_{12},s_{23},s_{13}) = c_{ggh}A^{(0)}_{h,ggg} + \sum_q c_q A^{(0)\lambda}_{q,ggg}(s_{12},s_{23},s_{13}) \tag{5.16}$$

with

$$A^{(0)}_{h,ggg} = 1. \tag{5.17}$$

Out of the eight possible helicity configurations, only two are independent, the others being related by parity and relabelings. They are given by

$$\mathcal{H}^{+++}(s_{12},s_{23},s_{13}) = \mathcal{H}^{---}(s_{12},s_{23},s_{13}) = \frac{m_h^8}{s_{12}s_{23}s_{13}}, \tag{5.18}$$

$$\mathcal{H}^{++-}(s_{12},s_{23},s_{13}) = \mathcal{H}^{--+}(s_{12},s_{23},s_{13}) = \mathcal{H}^{+-+}(s_{23},s_{13},s_{12}) = \mathcal{H}^{-+-}(s_{23},s_{13},s_{12}) = \mathcal{H}^{-++}(s_{13},s_{12},s_{23}) = \mathcal{H}^{+--}(s_{13},s_{12},s_{23}) = \frac{s_{12}^3}{s_{23}s_{13}}. \tag{5.19}$$

The quark-loop functions $A^{(0)\lambda}_{q,ggg}$ read

$$A^{(0)+++}_{q,ggg}(s_{12},s_{23},s_{13}) = A^{(0)---}_{q,ggg}(s_{12},s_{23},s_{13}), \tag{5.20}$$

$$A^{(0)++-}_{q,ggg}(s_{12},s_{23},s_{13}) = A^{(0)--+}_{q,ggg}(s_{12},s_{23},s_{13}) = A^{(0)+-+}_{q,ggg}(s_{23},s_{13},s_{12}) = A^{(0)-+-}_{q,ggg}(s_{23},s_{13},s_{12}) = A^{(0)-++}_{q,ggg}(s_{13},s_{12},s_{23}) = A^{(0)+--}_{q,ggg}(s_{13},s_{12},s_{23}) \tag{5.21}$$

and can be found in the literature; see Table V.

TABLE V. References for the two independent helicity amplitudes for the quark-loop contribution to the ggg channel, including the relations of their expressions to our notation. In [3], $\Delta = \sqrt{s_{12}s_{23}s_{13}/8}$ is defined and a sign flip for the parity transformed amplitude $\mathcal{M}_{-\lambda}$ is introduced, which is not reflected by (5.20) and (5.21), and instead absorbed into the square root of $\mathcal{H}^\lambda$. It drops out after squaring the amplitude. In [39], the spinor-helicity formalism [40–44] is employed using the convention $\langle ij\rangle[ji] = s_{ij}$.

Reference	$A^{(0)+++}_{q,ggg}(s_{12},s_{23},s_{13})$	$A^{(0)++-}_{q,ggg}(s_{12},s_{23},s_{13})$
[45]	$-2A_4(s_{12},s_{23},s_{13})$	$-2\frac{m_h^4}{s_{12}^2}A_2(s_{12},s_{23},s_{13})$
[3]	$\frac{s_{12}s_{23}s_{13}}{m_h^4}\frac{m_f^2}{16}\frac{\mathcal{M}_{++-}}{m_f^2\Delta}$	$-\frac{s_{23}s_{13}}{s_{12}}\frac{m_f^2}{16}\frac{\mathcal{M}_{+++}}{m_f^2\Delta}$
[39]	$-i(4\pi)^2 v\frac{\langle 12\rangle\langle 23\rangle\langle 31\rangle}{m_h^4}A_4^f(1^+,2^+,3^+,H)$	$i(4\pi)^2 v\frac{[23][31]}{[12]^3}A_4^f(1^+,2^+,3^-,H)$

2. $h \to gq\bar{q}$ channel

Denoting the outgoing gluon, quark and antiquark momenta by p_1, p_q and $p_{\bar{q}}$, respectively, and defining the Mandelstam variables s_{ij} as before with $s_{q\bar{q}}+s_{1q}+s_{1\bar{q}}=m_h^2$, the contribution of the $gq\bar{q}$ channel, for a single massless quark flavor, to the NLO decay rate is given by

$$\Gamma^{R,gq\bar{q}}_{h\to gg} = \frac{\alpha_s^3}{4\pi m_h v^2}(N_c^2-1)\int \mathrm{d}\Phi_3(p_1,p_q,p_{\bar{q}})\frac{s_{1q}^2+s_{1\bar{q}}^2}{s_{q\bar{q}}} \times \left|A^{(0)}_{h\to gq\bar{q}}(s_{q\bar{q}},s_{1q},s_{1\bar{q}})\right|^2. \tag{5.22}$$

We already carried out the helicity sum, as the function

$$A^{(0)}_{h\to gq\bar{q}}(s_{q\bar{q}},s_{1q},s_{1\bar{q}}) = c_{ggh}A^{(0)}_{h,gq\bar{q}} + \sum_q c_q A^{(0)}_{q,gq\bar{q}}(s_{q\bar{q}},s_{1q},s_{1\bar{q}}) \tag{5.23}$$

is helicity independent. The normalization is again chosen such that for the tree-level contribution

$$A^{(0)}_{h,gq\bar{q}} = 1. \tag{5.24}$$

The relevant expressions for the quark-loop function can again be found in the literature; see Table VI.

C. Implementation and validation

We implemented the calculation of the $h \to gg$ decay rate as a C++ program. For the real radiation phase space integration we used the Monte Carlo algorithm SUAVE, implemented in the CUBA library [46]. Infrared phase space singularities and the cancellation of infrared poles of the virtual correction matrix elements are handled by means of the antenna subtraction method [33–35]; see Appendix A. We use the CRunDec package [47–49] to obtain the numerical value of the running strong coupling in the $N_F = 5$ scheme at the two-loop level. If required, the same package can also be used to convert between the different quark mass schemes of Eqs. (3.8) and (3.10).

We validated our implementation by checking the individual ingredients and stages of the calculation:

Validation of the amplitudes.—We have recalculated all amplitudes except the two-loop NLO virtual SM contributions. Our analytic formulas agree with the ones given in the literature. Furthermore, after recovering the ordinary SM amplitudes by setting the effective couplings to their appropriate values, $c_{ggh}=0$ and $c_t=c_b=1$, we compared the squared one-loop Born and real correction amplitudes to their numerical counterparts obtained from OpenLoops2 [50], evaluated at a set of random phase space points. We found agreement within machine precision. OpenLoops2 also provides the relevant tree-level and one-loop amplitudes for $h \to gg$ at NLO QCD in the heavy-top limit, so that we could validate all amplitudes with effective hgg vertex setting $c_t=c_b=0$ and $c_{ggh}=\frac{2}{3}(1+11\frac{\alpha_s}{4\pi})$ [4].[4] We are not aware of any numerical implementation of the two-loop amplitude, against which we could compare in the same way. The references displayed in Table IV are in fact numerically self-consistent. However, only [38] contains the unrenormalized amplitudes, for which we have explicitly carried out the renormalization procedure.

Validation of the infrared subtraction.—Because of the simple infrared structure of the process and the fact that the decay $h \to gg$ in the limit of infinite top mass is actually used to derive the gluon-gluon antenna functions [51], we can check by hand that the infrared poles of the virtual correction amplitudes are correctly canceled. We confirmed the cancellation numerically as a test of our implementation. In order to validate the proper functioning of the real subtraction, we checked numerically that the ratio between real radiation matrix elements and the subtraction term tends to unity as we probe regions of the phase space ever closer to IR singular configurations. For the actual phase space integration, we implemented a cut parameter preventing the integrator to probe regions close to the singularity where cancellations between a very large matrix element and subtraction term occur. Those cancellations can escape the numerical precision leading to instabilities. The value of this cut must be chosen small enough so that only regions of the phase space are cut out in which the matrix element and the subtraction term can be treated as equal, leading to a vanishing contribution to the full integral. The final result should then not depend on small variations of the cut parameter. We checked that this is indeed the case.

Validation of the decay rate.—The code is structured such that we can vary the effective couplings at will. By setting them to the appropriate values, we can therefore calculate the $h \to gg$ decay rate up to NLO QCD either with full m_t dependence or in the limit of infinite top mass.[5]

TABLE VI. References for the quark-loop amplitudes contributing to the $gq\bar{q}$ channel and relations to the corresponding expressions therein.

Reference	$A^{(0)}_{q,gq\bar{q}}(s_{q\bar{q}},s_{1q},s_{1\bar{q}})$
[45]	$\frac{m_h^2}{m_h^2-s_{q\bar{q}}}A_5(s_{q\bar{q}},s_{1q},s_{1\bar{q}})$
[3]	$\frac{2}{m_h^2-s_{q\bar{q}}}\mathcal{A}(s_{q\bar{q}},s_{1q},s_{1\bar{q}})$

[4]Note that expanding c_{ggh} in terms of the strong coupling interferes with the perturbative expansion of the $h \to gg$ amplitude. The only place where the additional term $11\frac{\alpha_s}{4\pi}$ is relevant at $\mathcal{O}(\alpha_s^3)$ is as a finite renormalization of the virtual corrections, proportional to the Born amplitude (see also Appendix B).

[5]The latter is achieved without actually sending $m_t \to \infty$, but rather by setting c_{ggh} to the value of the effective coupling in the heavy-top limit, see footnote 4.

TABLE VII. Values of the LO and NLO coefficients. The parametric uncertainty is derived by varying the input parameters, the scale uncertainty by varying the renormalization scale μ_R by factors of 0.5 and 2.

	LO			NLO		
Coefficient	Value [MeV]	Parametric uncertainty (%)	Scale uncertainty (%)	Value [MeV]	Parametric uncertainty (%)	Scale uncertainty (%)
A_{gg}	0.41360	±1.5	$^{+23}_{-17}$	0.59755	±1.7	$^{+9.5}_{-9.6}$
A_{tt}	0.19595	±1.5	$^{+23}_{-17}$	0.32290	±1.8	$^{+13}_{-11}$
$A_{tt} + \delta A_{tt}$				0.32468	±1.8	$^{+13}_{-12}$
A_{bb}	0.00218	±4.0	$^{+23}_{-17}$	0.00328	±4.0	$^{+11}_{-10}$
A_{tg}	0.56937	±1.5	$^{+23}_{-17}$	0.88041	±1.8	$^{+11}_{-11}$
A_{bg}	−0.03442	±2.0	$^{+23}_{-17}$	−0.04837	±2.2	$^{+8.8}_{-9.2}$
A_{bt}	−0.02369	±2.0	$^{+23}_{-17}$	−0.03569	±2.2	$^{+11}_{-10}$

We checked that for both cases we can reproduce the numerical results known from the literature [4] within uncertainties. As a consistency check we confirmed that when setting c_{ggh} to the heavy-top limit value, c_t to 1 and sending $m_t \to \infty$, the rate tends to 4 times the rate in the heavy-top limit, as expected. This tests the relative phase between the c_{ggh} term and the quark-loop amplitudes. The $h \to gg$ rate including a local hgg vertex has been implemented previously in the program eHDECAY [28] considering QCD effects up to N^{3}LO in the limit of heavy fermion masses. The exact dependence on the top and bottom mass is included up to NLO in the pure fermion loop contributions, corresponding to our coefficients A_{tt}, A_{bb} and A_{bt}. eHDECAY also takes the charm quark into account, which we neglected in our numerical studies due to its small overall impact. In order to compare with eHDECAY we included it as well. Checking different settings for the effective couplings c_i we observe between 5% and 12% smaller rates obtained with our code, which can be attributed to the missing higher order QCD effects in our implementation. This discrepancy, however, is fully covered by the NLO scale uncertainty (see Sec. VI). Using additional information on the higher order effects in the heavy fermion mass limit from [52–57], we can supplement the results from our code with those effects, obtaining the rate at the same order in QCD as eHDECAY. Doing so we find agreement with eHDECAY for all tested configurations of effective couplings.

VI. PHENOMENOLOGICAL RESULTS FOR $h \to gg$

The coefficients A_i introduced in Eqs. (4.4) and (5.2) can be obtained by calculating the rate for six different combinations of coupling values and solving a simple system of linear equations, yielding

$$A_{gg} = \Gamma_{h\to gg}|_{c_{ggh}=1,c_t=0,c_b=0}, \tag{6.1}$$

$$A_{tt} = \Gamma_{h\to gg}|_{c_{ggh}=0,c_t=1,c_b=0}, \tag{6.2}$$

$$A_{bb} = \Gamma_{h\to gg}|_{c_{ggh}=0,c_t=0,c_b=1}, \tag{6.3}$$

$$A_{tg} = \Gamma_{h\to gg}|_{c_{ggh}=1,c_t=1,c_b=0} - A_{gg} - A_{tt}, \tag{6.4}$$

$$A_{bg} = \Gamma_{h\to gg}|_{c_{ggh}=1,c_t=0,c_b=1} - A_{gg} - A_{bb}, \tag{6.5}$$

$$A_{bt} = \Gamma_{h\to gg}|_{c_{ggh}=0,c_t=1,c_b=1} - A_{tt} - A_{bb}. \tag{6.6}$$

We compute the coefficients using the input parameters shown in Table II, treating the charm quark as massless, i.e. neglecting the decay of the Higgs through charm quark loops. In the SM this contribution accounts for less than 3% of the rate.

Table VII shows the results for LO and NLO QCD together with the value of the coefficient A_{tt}^{NLO} shifted by

$$\delta A_{tt}^{\mathrm{NLO}} = \left(\frac{\alpha_s}{4\pi}\right)^4 \frac{242}{9\pi}\frac{m_h^3}{v^2} \quad (\text{for } N_c = 3). \tag{6.7}$$

Formally this contribution is part of the NNLO corrections. It should, however, not be neglected, because it is effectively the dominant contribution to the rate close to specific values of the couplings c_{ggh}, c_t and c_b for which the LO and NLO amplitudes are parametrically suppressed, but the higher order corrections are not. In these regions of the parameter space the rate truncated at $\mathcal{O}(\alpha_s^3)$ can even become negative and thus unphysical. It is important to distinguish these configurations from a parametric suppression where simply all couplings are chosen to be small, which would affect the rate at all orders in a similar way.

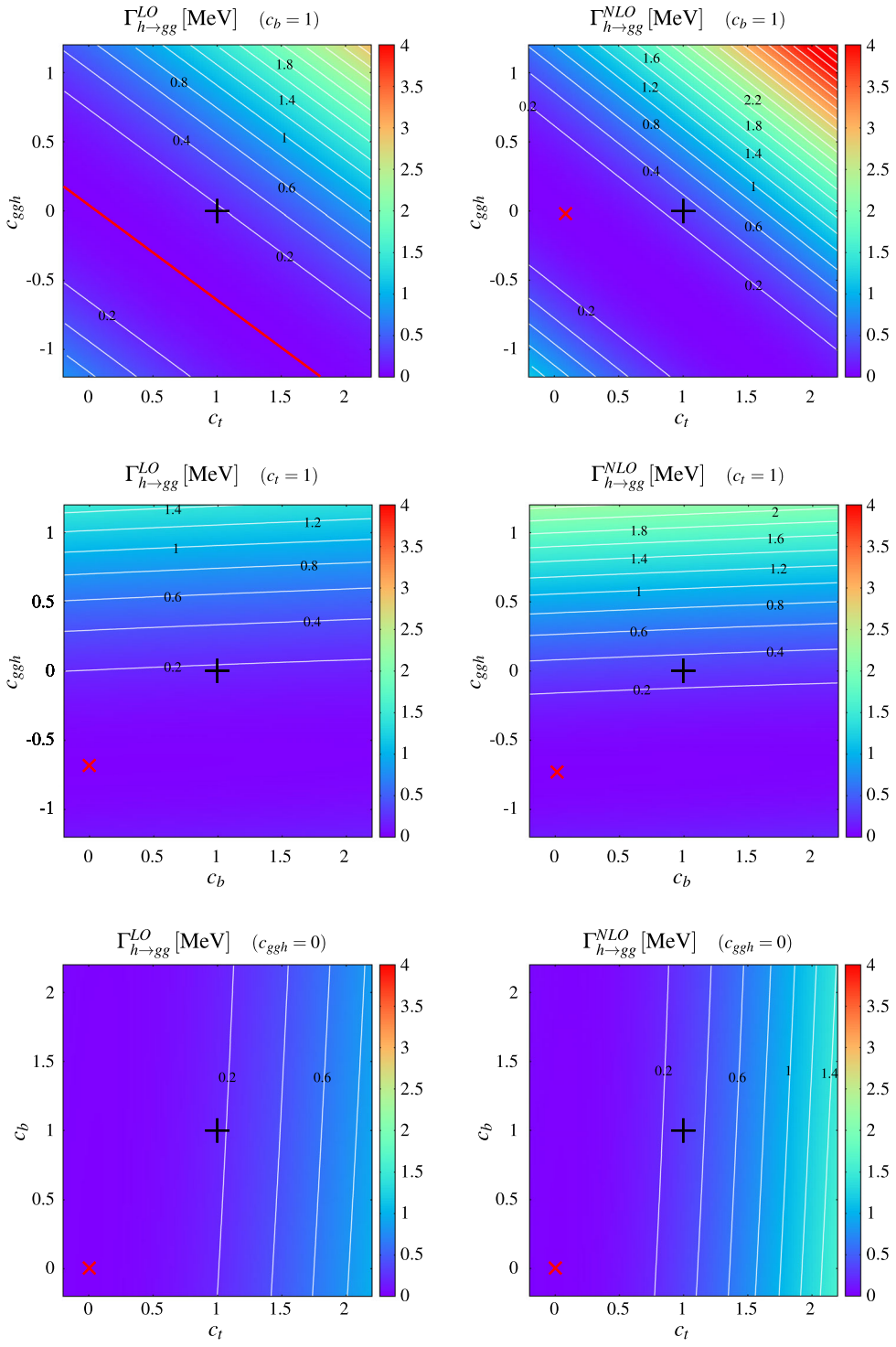

FIG. 8. Contour plots of the $h \to gg$ LO (left) and NLO (right) decay rates for different values of the effective couplings. The SM configuration is marked with a black cross at the center of the plots. A red cross shows the global minimum. In the upper left panel, LO for fixed $c_b = 1$, the global minimum is not a single point but rather a line.

We will include the shift in all our NLO plots in order to get more reliable predictions in these regions of the parameter space. One should keep in mind that these predictions are effectively of lower order in perturbation theory and are subject to larger uncertainties compared to the rate away from any parametric suppression, where the usual perturbative expansion holds and the phenomenological impact of the shift is small. In Appendix B, we motivate and derive Eq. (6.7) in more detail.

Besides the numerical values of the coefficients, we also give their respective scale and parametric uncertainties.[6] The former is obtained from varying the renormalization scale μ_R by factors of 0.5 and 2 around its central value, which we choose to be $\mu_R = m_h$. The scale uncertainty serves as an estimate of the impact of missing higher order corrections, as the all-order result must be scale independent.

The parametric uncertainty is derived by varying the input parameters within their respective errors. Treating them as uncorrelated, we change one at a time while keeping all others fixed and eventually sum the individual variations, which are approximately symmetric, in quadrature. It is important to notice that the resulting parametric uncertainties on the coefficients A_i are correlated. The corresponding correlation matrix is given in Appendix C. For all coefficients but A_{bb} the uncertainty on the value of the strong coupling $\alpha_s(m_Z)$ has the largest impact. The uncertainty on A_{bb} is driven mainly by that on m_b, which also has small impact on A_{bg} and A_{bt}. The uncertainties of the other input parameters are negligible in comparison.

Using the results for the coefficients in Table VII and Eqs. (4.4) and (5.2) for the LO and NLO decay rates, respectively, we can now determine the rate for arbitrary values of the effective couplings. For the SM case ($c_{ggh} = 0$, $c_t = c_b = 1$) we find

$$\Gamma^{\mathrm{LO,SM}}_{h\to gg} = (0.1744 \pm 1.5\%(\mathrm{param})^{+23\%}_{-17\%}(\mathrm{scale}))\ \mathrm{MeV}, \quad (6.8)$$

$$\Gamma^{\mathrm{NLO,SM}}_{h\to gg} = (0.2923 \pm 1.8\%(\mathrm{param})^{+13\%}_{-12\%}(\mathrm{scale}))\ \mathrm{MeV}. \quad (6.9)$$

The contribution of the shift (6.7) to the NLO rate is less than 1%. It is included in (6.9).

The contribution of the bottom-quark loops, entering through A_{bb}, A_{bt} and A_{bg} is small, but non-negligible compared to the largest SM contribution A_{tt}, the top-quark loop. Indeed, the bottom loop interferes destructively with the top loop and decreases the decay rate by about 10% compared to the top-only case, both at LO and NLO.

The coefficients related to the local Higgs-gluon interaction, A_{gg}, A_{tg} and A_{bg}, are comparatively large. In particular we observe a strong interference between the local and top loop contribution. This renders the rate very sensitive to not only the effective coupling c_{ggh}, but also the ratio c_{ggh}/c_t.

We can confirm these findings graphically by plotting heat maps of the decay rate, varying two of the effective couplings around their SM values, while keeping the third fixed at its SM value. Figure 8 shows the LO (left panels) and NLO (right panels) rates. The SM configuration $c_{ggh} = 0$, $c_t = c_b = 1$ always lies at the center and is marked with a black cross. In addition we highlighted the global minimum with a red cross. At LO it is given by

$$\Gamma^{\mathrm{LO}}_{h\to gg}|_{\mathrm{min}} = c_b^2 \left(\frac{\alpha_s}{4\pi}\right)^2 \frac{N_c^2 - 1}{64\pi} \frac{m_h^3}{v^2} (\mathrm{Im}\{A_q^{(0)}(\tau_b)\})^2, \quad (6.10)$$

and is located where the real part of the LO amplitude (4.2) vanishes, i.e.

$$c_{ggh} A_h^{(0)} + \frac{1}{2} c_t A_q^{(0)}(\tau_t) + \frac{1}{2} c_b \mathrm{Re}\{A_q^{(0)}(\tau_b)\} = 0. \quad (6.11)$$

Here we made use of the fact that $A_h^{(0)}$ and $A_q^{(0)}(\tau_t)$ [Eqs. (4.3) and (3.5)] are real and only $A_q^{(0)}(\tau_b)$ has an imaginary part. Consequently, the global minimum in the upper left panel, LO with $c_b = 1$ fixed, is not a single point, but rather a line. Close to the minimum, both the LO and NLO rates are much smaller than the rates for the SM like configuration, (6.8) and (6.9), due to the parametric suppression discussed above. This can also be seen in Fig. 9, where the LO and NLO decay rates, normalized to c_t^{-2}, as a function of the ratio c_{ggh}/c_t of the effective couplings are shown. The scale uncertainty reduces when going from LO to NLO, but the scale bands do not overlap, hinting towards a slow convergence of the perturbative series. This suggests that the calculation of NNLO corrections might be needed to get a more reliable theory estimate of the decay rate. We remark that in the region of parametric

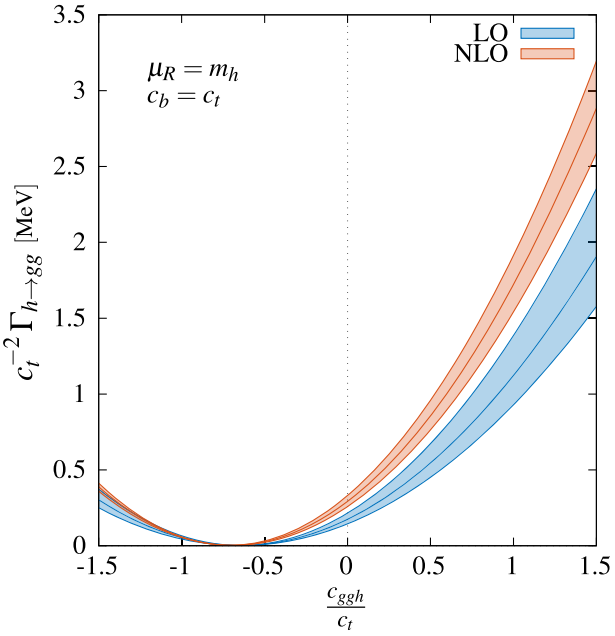

FIG. 9. Inclusive decay rate $\Gamma_{h\to gg}$, rescaled by c_t^{-2}, as a function of the ratio c_{ggh}/c_t of the effective couplings. The error bands are obtained through scale variation.

[6]The Monte Carlo error from the numerical phase space integration is several orders of magnitude smaller than those uncertainties.

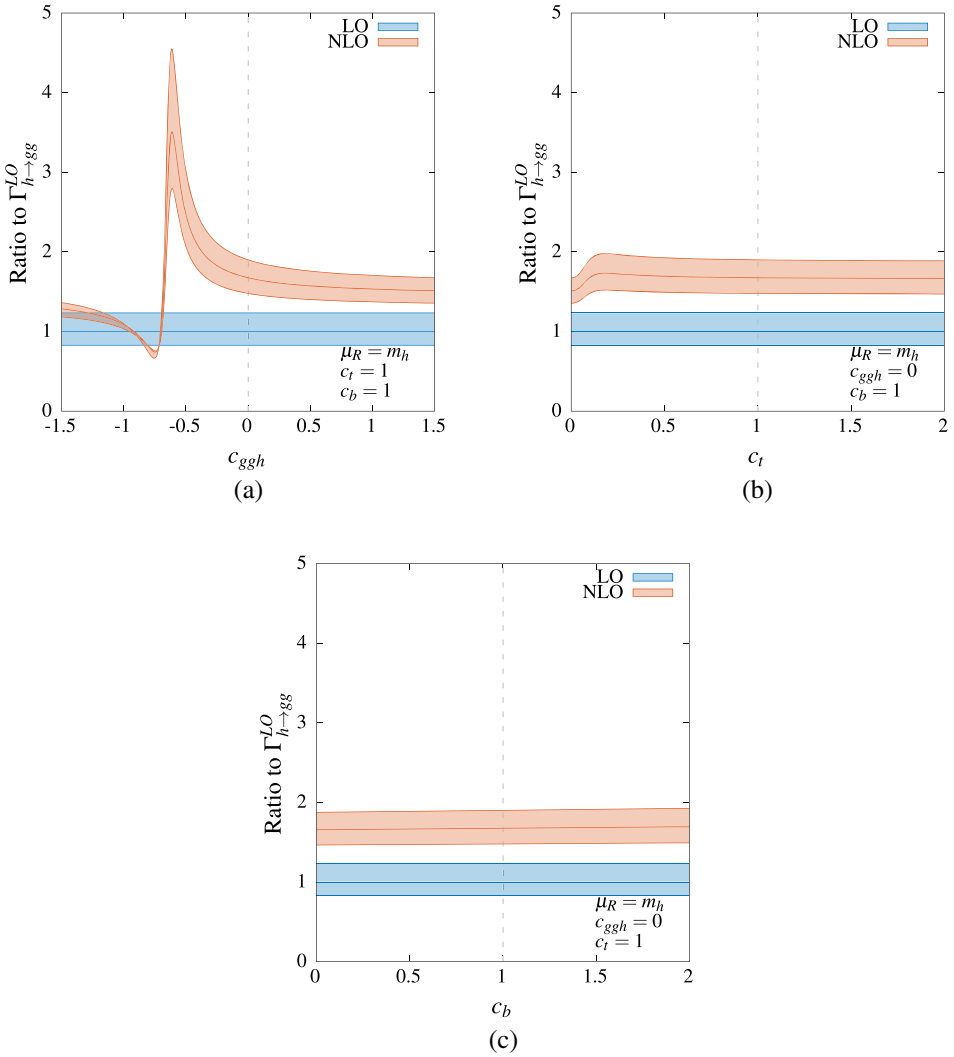

FIG. 10. Dependence of the QCD K-factor on the values of the effective couplings. In each panel, one coupling is varied while the other two are kept at their respective SM values. Again, the error bands are obtained through scale variation. The denominator $\Gamma^{\mathrm{LO}}_{h\to gg}$ is fixed to the central scale $\mu_R = m_h$.

suppression of the rates, the scale variation is not a good measure for the theory uncertainty: the underlying assumption that consecutive terms in the perturbative expansion decrease in magnitude is not fulfilled.

The effect of the NLO corrections can also be studied by plotting the QCD K-factor, i.e. the ratio $\Gamma^{\mathrm{NLO}}_{h\to gg}/\Gamma^{\mathrm{LO}}_{h\to gg}$, as a function of the effective couplings c_{ggh}, c_t and c_b. In Fig. 10 we show the K-factor, varying one coupling at a time and fixing the others at their respective SM values. The denominator is evaluated at the central scale $\mu_R = m_h$, while in the numerator μ_R is varied as previously by factors of 0.5 and 2. We also show the LO in blue, so that we can easily compare the scale uncertainty to the magnitude of the shift induced by the QCD corrections. The SM like configuration is indicated with a dashed line. We again see that the bands mostly do not overlap, pointing towards the necessity of higher order corrections to be included.

Figure 10(a) shows the K-factor for $c_t = c_b = 1$ as a function of c_{ggh}. For $c_{ggh} > 0$, the QCD corrections increase the rate by about 60%, with only a modest dependence on c_{ggh}, whereas for $c_{ggh} < 0$, in particular close to $c_{ggh} \approx -0.7$, the K-factor shows a highly nontrivial behavior. Here the effect of the parametric suppression of the LO rate can be seen. As explained above, the scale band of the NLO result underestimates the true uncertainty at this point.

Figure 10(b) captures the dependence on c_t for $c_b = 1$ and $c_{ggh} = 0$. The K-factor is almost flat, showing an increment of the rate of about 70%. Close to $c_t = 0$ the K-factor slightly drops. Here the destructive interference between the top and bottom loop is enhanced, with an effect similar to what we saw in the previous plot, just less pronounced.

The last plot, Fig. 10(c), shows the K-factor as a function of c_b, for $c_t = 1$ and $c_{ggh} = 0$. In accordance with the small

TABLE VIII. Definition of the anomalous couplings c_i in (2.6) in terms of the fundamental parameters of the EWChL defined in Sec. I and Ref. [11] and the Warsaw basis Wilson coefficients C_i.

Coupling	EWChL	Warsaw basis
c_f	$\frac{\mathcal{M}_{f,1}}{m_f}$	$1+\frac{v^2}{\Lambda^2}C_{\varphi\Box}-\frac{v^2}{4\Lambda^2}C_{\varphi D}-\frac{v^3}{\sqrt{2}m_f\Lambda^2}C_{f\varphi}$
c_V	$\frac{F_1}{2}$	$1+\frac{v^2}{\Lambda^2}C_{\varphi\Box}-\frac{v^2}{4\Lambda^2}C_{\varphi D}$
c_{ggh}	$16\pi^2 f_{Xh3,1}$	$\frac{32\pi^2v^2}{g_s^2\Lambda^2}C_{\varphi G}$
$c_{\gamma\gamma h}$	$16\pi^2(2f_{Xh1,1}+f_{Xh2,1}+f_{XU1,1})$	$\frac{32\pi^2v^2}{\Lambda^2}\left(\frac{C_{\varphi W}}{g^2}+\frac{C_{\varphi B}}{g'^2}-\frac{C_{\varphi WB}}{gg'}\right)$

overall contribution from the bottom-quark amplitude, we see a negligible dependence of the K-factor on c_b in this parameter range.[7] Going from LO to NLO increases the rate by approximately 70%.

In the figures we discussed we allow $\mathcal{O}(1)$ deviations of the effective couplings c_{ggh}, c_t and c_b from their respective SM values. A global fit [58] of the parameters of the EWChL to Higgs-boson signal strength measurements at the LHC shows that only deviations of $\mathcal{O}(0.1)$ are allowed by data, neglecting a few configurations of the couplings which are deemed unnatural in the context of the EFT approach. The fit in [58] has been performed at LO in QCD, with the exception of approximate NLO effects in the top quark contribution to the $h \to \gamma\gamma$ and $h \to gg$ decay rates, in the $m_t \to \infty$ limit. With our calculation we provide one ingredient to extend such a fit to include full NLO QCD effects.

VII. RESULTS FOR $h \to gg$ AND $h \to \gamma\gamma$ IN SMEFT

The previous discussion was based on the anomalous couplings in the context of the EWChL, which parametrizes the Higgs sector in a nonlinear manner and is particularly suited for Higgs-related Beyond-the-Standard-Model (BSM) scenarios with strong coupling dynamics. However, the results presented in this work are actually applicable to a broad variety of situations.

A common extrapolation of the SM into the UV regime consists in adding higher dimensional operators to the dimension-four SM, resulting in the SMEFT. We restrict ourselves to the leading corrections from operators of canonical dimension six. Here, the electroweak symmetry breaking pattern is realized in a linear manner and the new physics (NP) can decouple from the SM allowing for a large mass gap. It is important to notice, however, that even in such general situations, the power counting is not as arbitrary as it seems at first glance. For instance, it is easy to construct explicit weakly coupled UV models that, when matched to dimension-six terms in the Warsaw basis [59], result in a hierarchy among operators of the same mass dimension. The clue lies in keeping track of explicit loop factors $1/16\pi^2$ arising in the full theory that can be hidden in the Wilson coefficients of certain local operators. A systematic power-counting prescription for SMEFT is therefore defined by canonical dimensions supplemented by a loop-counting rule, allowing us to keep track of the loop expansion, on which perturbative calculations in quantum field theory are based [60].

For our purpose, the most significant implication is that operators featuring field strength tensors (e.g. the operator[8] $Q_{\varphi G}$) are suppressed with an extra loop factor when compared to the remaining ones. The formalism of the EWChL in (2.6) already accounts for loop factors in modified vertices involving the Higgs boson and can hence be taken over to SMEFT straightforwardly,[9] see Table VIII. The coefficients c_i can naturally be taken as $\mathcal{O}(1)$ numbers. As a consequence, setting $\Lambda = 1$ TeV, we have for instance $C_{\varphi G} \approx 0.08 c_{ggh}$, which makes the implicit loop factor in the definition of $C_{\varphi G}$ manifest. For further comments about the applicability of this Table, see [62].

In contrast, operators that induce anomalous couplings without the Higgs boson (e.g. the chromomagnetic operator Q_{uG}) are present within this framework only at subleading order. They can be neglected consistently without spoiling the underlying systematics. Similar arguments hold true for four-fermion operators. Despite appearing with unsuppressed Wilson coefficients, the relevant diagrams are of an explicit two-loop topology and can thus be dropped, see Fig. 11 for $h \to gg$.

Let us emphasize that in the context of NP in the Higgs sector and in particular when considering the Higgs decay channels highlighted in this paper, it is advantageous to work with the EWChL, independently of the actual high energy dynamics being strongly or weakly coupled to the SM. While the difference between the EWChL and SMEFT is less apparent when restricting the latter to canonical dimension six, it becomes more relevant when higher dimensional operators are considered. For instance, the impact of a generic $(2n+4)$-dimensional operator $(\varphi^\dagger\varphi)^n G^a_{\mu\nu} G^{a\mu\nu}$ to

[7] We see a slightly increased dependence if we enlarge the parameter range of c_b to $\pm\mathcal{O}(10)$.

[8] Here and in the following, we employ the notation of [61].

[9] The EWChL can account for strong coupling scenarios in the gauge boson sector pushing the first deviations from the SM, parametrized by F_1, formally to the LO. This is not the case for weak coupling scenarios which are conveniently handled by SMEFT.

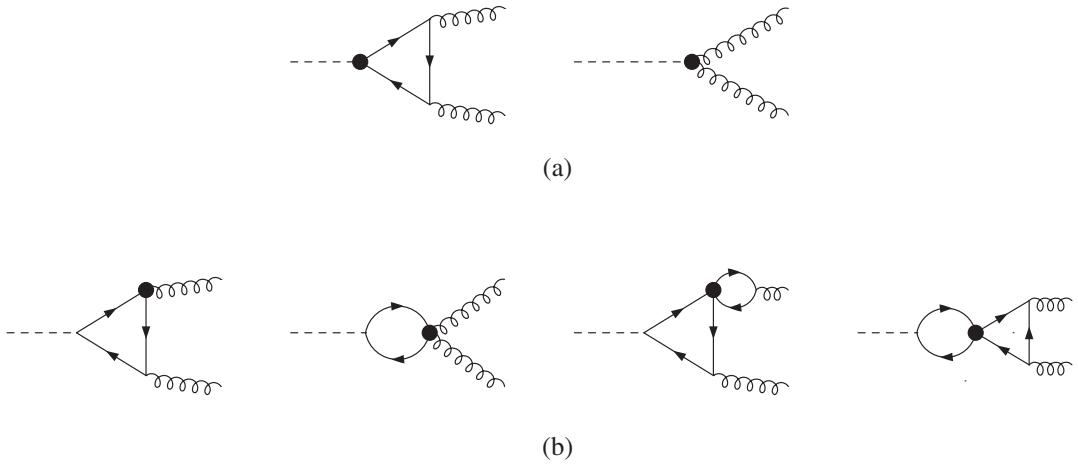

FIG. 11. Diagrams contributing to $h \to gg$ in SMEFT with single dimension-six insertions (black dots). (a) Contributions of order $\sim g_s^2/16\pi^2$ with anomalous couplings defined in Table VIII. (b) Contributions of order $\sim g_s^2/(16\pi^2)^2$ that can consistently be neglected. This qualitative picture can be taken over to the process $h \to \gamma\gamma$.

the local Higgs-gluon-gluon interaction in SMEFT is already accounted for by c_{ggh} within the EWChL. While SMEFT has contributions at all orders in the $1/\Lambda$ expansion, only a single coefficient is responsible in the EWChL. An explicit distinction between the various $1/\Lambda^{2n}$ terms that eventually sum up to c_{ggh} is not necessary at this stage as it would increase the number of independent parameters, complicating the exploration of NP effects, which are yet to be discovered. Based on the idea of organizing the Higgs-field factors $(\varphi^\dagger\varphi)^n$ in higher dimensional operators, the framework of geoSMEFT has been developed [63], for which an analysis of $h \to gg$ can be found in [64,65].

In the language of the EWChL and working at NLO in QCD we have

$$\frac{\Gamma^{\rm EWChL}_{h\to gg}}{\Gamma^{\rm SM}_{h\to gg}} = 1 + 2\,\delta_{c_t} + 2.7116\,c_{ggh} + \delta_{c_t}^2 + 1.8404\,c_{ggh}^2 + 2.7116\,\delta_{c_t} c_{ggh}, \tag{7.1}$$

where we defined $\delta_{c_t} \equiv c_t - 1$. Employing the relations of Table VIII, it is straightforward to obtain a numerical expression for SMEFT up to operator dimension six and NLO in QCD. Defining $\tilde{C}_i \equiv C_i v^2/\Lambda^2$, we find

$$\begin{aligned}\frac{\Gamma^{\rm SMEFT}_{h\to gg}}{\Gamma^{\rm SM}_{h\to gg}} &= 1 + 2\left(\tilde{C}_{\varphi\Box} - \frac{1}{4}\tilde{C}_{\varphi D}\right) - 2.0164\tilde{C}_{t\varphi} + 578.04\tilde{C}_{\varphi G} \\ &\quad + \left(\tilde{C}_{\varphi\Box} - \frac{1}{4}\tilde{C}_{\varphi D}\right)^2 - 2.0164\left(\tilde{C}_{\varphi\Box} - \frac{1}{4}\tilde{C}_{\varphi D}\right)\tilde{C}_{t\varphi} \\ &\quad + 1.0164\tilde{C}_{t\varphi}^2 + 8.3632\times 10^4\tilde{C}_{\varphi G}^2 \\ &\quad + 578.04\left(\tilde{C}_{\varphi\Box} - \frac{1}{4}\tilde{C}_{\varphi D}\right)\tilde{C}_{\varphi G} - 582.77\tilde{C}_{t\varphi}\tilde{C}_{\varphi G}.\end{aligned} \tag{7.2}$$

Note that this expression is not fully systematic. First, it retains only a part of the $\mathcal{O}(1/\Lambda^4)$ correction to the SM, since dimension-eight operators are not included, in contrast to the general form (7.1). This can be improved by extending the relations of Table VIII to higher canonical dimensions. For example, dimension-eight contributions to (7.2) can be found in [64,65] (minor numerical differences arise due to a somewhat different treatment of higher order corrections). Second, it hides the possible implicit loop factor hidden in the coefficient $C_{\varphi G}$. A superficial inspection of (7.2) would therefore lead to expect the highest deviations to be associated with this operator. As stated before, adding a consistent power-counting prescription for loops to the usual canonical counting in SMEFT can resolve this issue [60]. For instance, the coefficient in front of $\tilde{C}_{\varphi G}$ would change from 578.04 to 3.6605, which is a number of order unity.

While in SMEFT the exact anomalous coupling between one Higgs boson and two gluons is given by an infinite tower of coefficients with increasing number of canonical dimension (and hence decreasing phenomenological importance), the formalism of the EWChL highlights the existence of a single anomalous coupling parameter c_{ggh}. It is therefore inconvenient to treat $C_{\varphi G}$ and its higher dimensional relatives $C_{\varphi G}^{(8)}$, $C_{\varphi G}^{(10)}$, etc. on unequal footing for single-Higgs processes. This also becomes clear in the context of QCD corrections. The latter can be summed up for all individual SMEFT contributions at once, which is equivalent to considering only one parameter from the start. Distinguishing contributions associated with different canonical dimensions is therefore not possible in the present case. For instance, $C_{\varphi G}$ and $C_{\varphi G}^{(8)}$ cannot be extracted individually in single-Higgs processes, no matter how precise the experimental measurement is. However, processes involving two or more external Higgs states need

additional coefficients, e.g. c_{gghh}. In SMEFT at canonical dimension eight, c_{ggh} and c_{gghh} are represented by different linear combinations of $C_{\varphi G}$ and $C^{(8)}_{\varphi G}$. Disentangling the latter coefficients thus requires the comparison of processes with a varying number of Higgs particles [10,62].

VIII. CONCLUSIONS

We have performed a detailed analysis of QCD corrections at NLO for the Higgs-boson decays $h \to gg$ and $h \to \gamma\gamma$, allowing for the presence of anomalous Higgs couplings from new-physics effects. The natural framework for this task is provided by the EWChL, which accounts for anomalous Higgs couplings at leading order in the EFT. In addition, the EFT is governed by a power counting in loop orders, which can be systematically combined with QCD perturbation theory.

For $h \to gg$ the relevant EFT coefficients are the local Higgs-gluon coupling c_{ggh}, the Higgs-top coupling c_t and, to a lesser extent, the Higgs-bottom coupling c_b. They are scale invariant under QCD. No additional EFT parameters arise when the QCD calculation is extended from LO to NLO. For the $h \to gg$ rate the impact of QCD is known to be large, with a K-factor of about 1.7. The uncertainties from scale dependence are reduced at NLO. This also holds for the case of anomalous couplings, in particular for the QCD coefficients of coupling factors, such as c_t^2, $c_t c_{ggh}$ or c_{ggh}^2, in the expression of the decay rate. Those coefficients show NLO scale uncertainties at the 10% level, reduced by about a factor of 2 compared to LO. QCD has less impact on $h \to \gamma\gamma$. In this case a NLO treatment of QCD effects practically eliminates uncertainties from perturbative QCD.

A new feature arising at NLO in QCD is that the analysis becomes sensitive to $\mathcal{O}(\alpha_s)$ corrections in the EFT coefficients c_{ggh} and $c_{\gamma\gamma h}$. Such terms are related to QCD corrections in the calculation of these coefficients from matching to the underlying UV completion of the EFT. In Appendix D we have illustrated this with several toy models for the UV physics.

We have also compared our treatment of the decays using the EWChL with a description based on SMEFT.

The results presented here provide the basis for a consistent determination of anomalous Higgs couplings from $h \to gg$ and $h \to \gamma\gamma$ at NLO in QCD.

ACKNOWLEDGMENTS

We thank Florian Pandler for useful discussions, and Michael Spira for valuable comments on the manuscript. This work was supported by the DFG, German Research Foundation, Grant No. BU 1391/2-2 (Project No. 261324988) and DFG, Germany's Excellence Strategy —EXC-2094–390783311 and Studienstiftung des deutschen Volkes. Ch. M.-S. was supported in part by a Fellowship of the Studienstiftung des deutschen Volkes (German Academic Scholarship Foundation).

APPENDIX A: IR SUBTRACTION

Consider the NLO decay rate (5.1):

$$\Gamma^{\mathrm{NLO}}_{h\to gg} = \Gamma^{\mathrm{LO}}_{h\to gg} + \Gamma^{V}_{h\to gg} + \Gamma^{R}_{h\to gg}. \tag{A1}$$

The V and R corrections are separately IR divergent, with V containing explicit poles in ϵ coming from loop integrals carried out in dimensional regularization, and R implicit phase space singularities related to soft or collinear final state particles. Summing both contributions, however, yields a finite result. In practice, the phase space integrals cannot be evaluated analytically for most processes and numerical integration methods have to be applied. In this case, the pole cancellation cannot be checked directly. In order to still obtain sensible results, one has to systematically regulate the integrand in regions of the phase space where it diverges. As stated before, we adopt the antenna subtraction formalism [33–35] for our setup, which proves to be particularly simple for the process at hand, i.e. $h \to gg$.

By construction the antenna subtraction term (S) reproduces the exact behavior of the real correction matrix element in the IR singular limits for each color level in the $1/N_c$ expansion individually. The difference of both can then be integrated numerically in a straightforward manner, as the integrand identically vanishes in all IR singular phase space regions. The subtraction term is constructed in such a way that, after appropriate factorization of the phase space, it can be integrated analytically over the phase space of the particle becoming unresolved. The integrated subtraction term (T) then exhibits explicit poles in ϵ which exactly cancel those of the virtual corrections. We have

$$\Gamma^{V}_{h\to gg} + \Gamma^{R}_{h\to gg} = \underbrace{\int_2 \mathrm{d}\Gamma^{V}_{h\to gg} - \int_2 \mathrm{d}\Gamma^{T}_{h\to gg}}_{\text{finite}} + \underbrace{\int_3 (\mathrm{d}\Gamma^{R}_{h\to gg} - \mathrm{d}\Gamma^{S}_{h\to gg})}_{\text{finite}}, \tag{A2}$$

where

$$\mathrm{d}\Gamma^{T}_{h\to gg} = -\int_{\mathrm{unres}} \mathrm{d}\Gamma^{S}_{h\to gg}. \tag{A3}$$

The IR-subtracted expression for the $h \to ggg$ channel (5.14) is given by

$$\int_3 (\mathrm{d}\Gamma^{R,ggg}_{h\to gg} - \mathrm{d}\Gamma^{S,ggg}_{h\to gg}) = \frac{\alpha_s^3}{24\pi m_h v^2} N_c(N_c^2-1)\int \mathrm{d}\Phi_3 \left(\sum_\lambda \mathcal{H}^\lambda |A^{(0)\lambda}_{h\to ggg}|^2 - 2m_h^4 F_3^0 |A^{(0)}_{h\to gg}|^2\right)$$
$$= \frac{\alpha_s^3}{24\pi m_h v^2} N_c(N_c^2-1)\int \mathrm{d}\Phi_3 \sum_\lambda \mathcal{H}^\lambda \left(|A^{(0)\lambda}_{h\to ggg}|^2 - |A^{(0)}_{h\to gg}|^2\right), \tag{A4}$$

where our special kinematics ($1 \to 3$ decay) allows for the F_3^0 antenna function [Eq. (7.8) in [33]] to be written as

$$m_h^4 F_3^0 = \frac{1}{2}\sum_\lambda \mathcal{H}^\lambda = \frac{m_h^8 + s_{12}^4 + s_{23}^4 + s_{13}^4}{s_{12}s_{23}s_{13}}. \tag{A5}$$

The IR-subtracted contribution of the $h \to gq\bar{q}$ channel (5.22) to the rate evaluates to

$$\int_3 (\mathrm{d}\Gamma^{R,gq\bar{q}}_{h\to gg} - \mathrm{d}\Gamma^{S,gq\bar{q}}_{h\to gg}) = \frac{\alpha_s^3}{4\pi m_h v^2}(N_c^2-1)\int \mathrm{d}\Phi_3 \left(\frac{s_{1q}^2 + s_{1\bar{q}}^2}{s_{q\bar{q}}} |A^{(0)}_{h\to gq\bar{q}}|^2 - m_h^4 G_3^0 |A^{(0)}_{h\to gg}|^2\right)$$
$$= \frac{\alpha_s^3}{4\pi m_h v^2}(N_c^2-1)\int \mathrm{d}\Phi_3 \frac{s_{1q}^2 + s_{1\bar{q}}^2}{s_{q\bar{q}}} \left(|A^{(0)}_{h\to gq\bar{q}}|^2 - |A^{(0)}_{h\to gg}|^2\right), \tag{A6}$$

where as before the G_3^0 antenna function [Eq. (7.14) in [33]] can be simplified yielding

$$m_h^4 G_3^0 = \frac{s_{1q}^2 + s_{1\bar{q}}^2}{s_{q\bar{q}}}. \tag{A7}$$

Adding back the (now integrated) subtraction term to the virtual contribution (5.7), we find

$$\Gamma^V_{h\to gg} - \Gamma^T_{h\to gg} = \frac{\alpha_s^3}{512\pi^4}\frac{m_h^3}{v^2}(N_c^2-1)(\mathrm{Re}\{A^{(0)\dagger}_{h\to gg} A^{(1)}_{h\to gg}\} + 2N_c \boldsymbol{J}_2^{(1)} |A^{(0)}_{h\to gg}|^2), \tag{A8}$$

where the integrated antenna string is given by

$$\boldsymbol{J}_2^{(1)} = \boldsymbol{J}_2^{(1),ggg} + \frac{N_F}{N_c}\boldsymbol{J}_2^{(1),gq\bar{q}} = \mu^{2\epsilon}\left(\frac{1}{3}\mathcal{F}_3^0(m_h^2) + \frac{N_F}{N_c}\mathcal{G}_3^0(m_h^2)\right). \tag{A9}$$

The integrated antenna functions $\mathcal{F}_3^0$ and $\mathcal{G}_3^0$ can be found in [33]. Explicitly,

$$\boldsymbol{J}_2^{(1)} = -\frac{1}{2N_c}\mathrm{Re}\left\{N_c I(\epsilon) - \beta_0 L + \frac{7}{3}N_F - \frac{73}{6}N_c\right\} + \mathcal{O}(\epsilon), \tag{A10}$$

where $L = \log\mu^2/m_h^2 + i\pi$ and $I(\epsilon)$ has been defined in (5.10). We thus find

$$\Gamma^V_{h\to gg} - \Gamma^T_{h\to gg} = \frac{\alpha_s^3}{512\pi^4}\frac{m_h^3}{v^2}(N_c^2-1)\left(\left(\beta_0 \log\frac{\mu^2}{m_h^2} - \frac{7}{3}N_F + \frac{73}{6}N_c\right)|A^{(0)}_{h\to gg}|^2 + \frac{1}{2}\sum_q c_q \mathrm{Re}\{A^{(0)\dagger}_{h\to gg} A^{(1)}_{q,g,\mathrm{fin}}(\tau_q)\}\right), \tag{A11}$$

which is finite as $\epsilon \to 0$.

APPENDIX B: PARAMETRIC SUPPRESSION OF THE DECAY RATE

In a theory in which the coupling of the Higgs to gluons is given by an effective local interaction, such as the c_{ggh} term in (2.6), the decay rate including $\mathcal{O}(\alpha_s)$ corrections can be given in exact form, as the integral over the phase space of the real radiation corrections can be calculated analytically. This is the case for the SM [4], considering only the top quark and the limit $m_t \to \infty$, in which the top-quark loop is no longer resolved, generating an effective Higgs-gluon interaction of the form $hG^a_{\mu\nu}G^{a\mu\nu}$.

The corresponding Wilson coefficient is known to N^{4}LO in QCD [8,54,55,57]. In this limit the relevant part of the effective Lagrangian (2.6) reduces to[10]

$$\mathcal{L}_{\text{eff}}^{\infty} \supset \frac{\alpha_s}{8\pi}\left(c_{ggh} + \frac{2}{3}c_t\left(1 + 11\frac{\alpha_s}{4\pi}\right)\right)\frac{h}{v}G^a_{\mu\nu}G^{a\mu\nu}, \tag{B1}$$

where the superscript "∞" indicates that we sent m_t to infinity. Since the heavy top limit is actually a very good approximation already at LO [4], this form of the Lagrangian enables us to explore the interplay of the effective couplings c_{ggh} and c_t in a simple, yet not unrealistic scenario. The decay rate reads

$$\Gamma^{\infty}_{h\to gg} = \Gamma^{\text{LO},\infty}_{h\to gg}\left[1 + \frac{\alpha_s}{\pi}\left(\mathcal{R} + \frac{11c_t}{3c_{ggh}+2c_t}\right) + \mathcal{O}(\alpha_s^2)\right], \tag{B2}$$

with

$$\Gamma^{\text{LO},\infty}_{h\to gg} = \left(\frac{\alpha_s}{4\pi}\right)^2 \frac{(3c_{ggh}+2c_t)^2}{18\pi}\frac{m_h^3}{v^2}, \tag{B3}$$

and

$$\mathcal{R} = \frac{73}{4} - \frac{7N_F}{6} + \frac{33-2N_F}{6}\log\frac{\mu_R^2}{m_h^2} \tag{B4}$$

is the finite contribution from the V and R corrections. The second term of the $\mathcal{O}(\alpha_s)$ correction is related to the $\mathcal{O}(\alpha_s)$ correction to the effective coupling, see (B1). For later convenience, we define

$$\Delta := \frac{11c_t}{3c_{ggh}+2c_t}. \tag{B5}$$

$c_{ggh} \approx -(2/3)c_t$ is obviously a critical region in the parameter space as the LO result (B3) becomes very small. While $\mathcal{R} > 0$ for realistic N_F and μ_R (i.e. $N_F = 5$ and $\mu_R \approx m_h$), the term Δ can become large and negative, eventually rendering the whole NLO decay rate unphysical when $1 + (\alpha_s/\pi)(\mathcal{R}+\Delta) < 0$. This is an artifact of neglecting a certain part of the $\mathcal{O}(\alpha_s^2)$ corrections—(B2) is not a perfect square—as we will explain in the following.

For $c_{ggh} = -(2/3)c_t$, both the LO and NLO rates vanish identically. The Higgs gluon coupling becomes effectively $\mathcal{O}(\alpha_s^2)$,

$$\mathcal{L}_{\text{eff}}^{\infty}\Big|_{c_{ggh}\to -\frac{2}{3}c_t} \supset \frac{\alpha_s^2}{32\pi^2}\frac{22c_t}{3}\frac{h}{v}G^a_{\mu\nu}G^{a\mu\nu}, \tag{B6}$$

and the rate starts at $\mathcal{O}(\alpha_s^4)$,

$$\Gamma^{\infty}_{h\to gg}\Big|_{c_{ggh}=-\frac{2}{3}c_t} = \left(\frac{\alpha_s}{4\pi}\right)^4 \frac{242c_t^2}{9\pi}\frac{m_h^3}{v^2} + \mathcal{O}(\alpha_s^5). \tag{B7}$$

This term is in fact a genuine part of the NNLO decay rate for arbitrary c_{ggh} and c_t. While the LO and NLO parts as well as the other NNLO pieces of the rate are parametrically suppressed for $c_{ggh} \approx -(2/3)c_t$, this one is not. It will be the dominant contribution to the decay rate in this regime, and should therefore not be neglected, irrespective of being formally of higher order in perturbation theory. We will thus define the NLO rate to include (B7),

$$\Gamma^{\text{NLO},\infty}_{h\to gg} = \Gamma^{\text{LO},\infty}_{h\to gg}\left[1 + \frac{\alpha_s}{\pi}(\mathcal{R}+\Delta)\right] + \left(\frac{\alpha_s}{4\pi}\right)^4 \frac{242c_t^2}{9\pi}\frac{m_h^3}{v^2} \tag{B8}$$

$$= \Gamma^{\text{LO},\infty}_{h\to gg}\left[\left(1 + \frac{\alpha_s}{\pi}\frac{\Delta}{2}\right)^2 + \frac{\alpha_s}{\pi}\mathcal{R}\right]. \tag{B9}$$

Δ now only appears in a square and the rate will always be positive for positive $\mathcal{R}$. For $c_{ggh} \approx -(2/3)c_t$, we will thus obtain a more reliable prediction, while for all other cases, the contribution of the Δ^2 term will be subdominant.

It turns out that the same parametric suppression of the LO and NLO rate occurs when we retain a finite top mass, namely in the region $c_{ggh} \approx -(c_t/2)A_q^{(0)}(\tau_t)$, see (4.2). This issue can again be resolved by adding (B7), which in fact is nothing but the $m_t \to \infty$ limit of the suitably IR-regulated part of the virtual corrections squared contribution to the NNLO corrections,[11]

$$\Gamma^{V\times V,\infty}_{h\to gg}|_{\text{IR-regulated}} = \left(\frac{\alpha_s}{4\pi}\right)^4 \frac{c_t^2}{2\pi}\left|\lim_{\tau_t\to 0} A^{(1)}_{q,g,\text{fin}}(\tau_t)\right|^2 \frac{m_h^3}{v^2} \tag{B10}$$

$$= \left(\frac{\alpha_s}{4\pi}\right)^4 \frac{242c_t^2}{9\pi}\frac{m_h^3}{v^2}, \tag{B11}$$

with $A^{(1)}_{q,g,\text{fin}}$ from Eq. (5.9). We will settle for the heavy top limit here, since the mass effects in this perturbatively suppressed term will be negligible for most of the parameter space, but remark that if one wishes to explore the parametrically suppressed region, i.e. close to the vanishing LO rate, one should keep in mind that the calculation is effectively a LO calculation in this specific approximation.

[10]See also Appendix D. Note that here we explicitly set $N_c = 3$.

[11]The double virtual corrections at the NNLO level consist of the interference of the Born amplitude with the amplitude with two additional loops, but also of the square of the amplitude with one additional loop. The IR divergences are compensated by double real and real virtual contributions.

In practice, this treatment amounts to a shift of the coefficient A_{tt}^{NLO} in the rate as defined in (5.2),

$$A_{tt}^{\mathrm{NLO}} \to A_{tt}^{\mathrm{NLO}} + \delta A_{tt}^{\mathrm{NLO}}, \tag{B12}$$

with

$$\delta A_{tt}^{\mathrm{NLO}} = \left(\frac{\alpha_s}{4\pi}\right)^4 \frac{242}{9\pi}\frac{m_h^3}{v^2}. \tag{B13}$$

This shift is contained in all plots in Sec. VI, where also the bottom-quark contribution is included. Figure 8 serves as an empirical check that the latter does not introduce any new critical points; the global minimum of the rate is positive for arbitrary values of c_{ggh}, c_t, and c_b.

We remark that this is in general not true if we include further light quarks, such as the charm. Albeit we expect its contribution [for $c_c \sim \mathcal{O}(1)$] to be comparatively small due to its small mass, it will be possible to find particular combinations in the now four-dimensional parameter space spanned by c_{ggh}, c_t, c_b, c_c for which the NLO rate will become negative, with very small magnitude. We checked for this particular scenario that it can only happen if c_b and c_c exceed c_t and c_{ggh} by at least 1 order of magnitude. Those configurations are well away from any region of phenomenological interest [58]. In addition, the argument that the predictions in these cases are effectively of lower order in perturbation theory still holds, and thus they are subject to larger uncertainties.

APPENDIX C: CORRELATIONS OF THE PARAMETRIC UNCERTAINTIES OF $\Gamma_{h\to gg}$

When calculating the parametric uncertainties of the decay rates Eq. (4.4) or Eq. (5.2), one has to take into account the correlations between the respective uncertainties σ_i of the coefficients A_i, as presented in Table VII. Those correlations are described by the symmetric matrix ρ, so that

$$\sigma_\Gamma = \sqrt{\sum_{i,k}\tilde{\sigma}_i\rho_{ik}\tilde{\sigma}_k} = \sqrt{\sum_i \tilde{\sigma}_i^2 + \sum_{i\neq k}\tilde{\sigma}_i\rho_{ik}\tilde{\sigma}_k}, \tag{C1}$$

where in case of the decay $h \to gg$ with anomalous couplings c_{ggh}, c_t, and c_b the vector $\tilde{\sigma}$ is defined as

$$\tilde{\sigma} = (c_{ggh}^2\sigma_{ggh}, c_t^2\sigma_{tt}, c_b^2\sigma_{bb}, c_t c_{ggh}\sigma_{tg}, c_b c_{ggh}\sigma_{bg}, c_b c_t \sigma_{bt}). \tag{C2}$$

At LO and NLO in QCD the correlation matrices read

$$\rho^{\mathrm{LO}} = \begin{pmatrix} 1 & 1.000 & 0.351 & 1.000 & -0.735 & -0.736 \\ 1.000 & 1 & 0.350 & 1.000 & -0.734 & -0.735 \\ 0.351 & 0.350 & 1 & 0.350 & -0.893 & -0.892 \\ 1.000 & 1.000 & 0.350 & 1 & -0.735 & -0.735 \\ -0.735 & -0.734 & -0.893 & -0.735 & 1 & 1.000 \\ -0.736 & -0.735 & -0.892 & -0.735 & 1.000 & 1 \end{pmatrix}, \tag{C3}$$

and

$$\rho^{\mathrm{NLO}} = \begin{pmatrix} 1 & 1.000 & 0.410 & 1.000 & -0.773 & -0.780 \\ 1.000 & 1 & 0.410 & 1.000 & -0.773 & -0.780 \\ 0.410 & 0.410 & 1 & 0.410 & -0.896 & -0.891 \\ 1.000 & 1.000 & 0.410 & 1 & -0.773 & -0.780 \\ -0.773 & -0.773 & -0.896 & -0.773 & 1 & 1.000 \\ -0.780 & -0.780 & -0.891 & -0.780 & 1.000 & 1 \end{pmatrix}, \tag{C4}$$

respectively. At the accuracy we are working at, the impact of the shift (6.7) on ρ^{NLO} is negligible.

APPENDIX D: TOY MODELS FOR $c_{\gamma\gamma h}$ AND c_{ggh}

The Lagrangian (2.6) provides an effective description of the physics around the scale of electroweak symmetry breaking v. Short distance effects related to the scale $f \gg v$ are encoded into the Wilson coefficients such as c_{ggh} and $c_{\gamma\gamma h}$. By experimentally constraining their values, one can make statements about the characteristics of the unknown high scale physics, as different models of the UV theory lead to different predictions for the size of the effective couplings. In the following we will consider two toy

models to sketch how the couplings c_{ggh} and $c_{\gamma\gamma h}$ are related to the parameters of the full theory, including $\mathcal{O}(\alpha_s)$ corrections.

In both scenarios, we consider a new heavy particle, colored and charged, mediating the coupling of the Higgs to photons and gluons through a loop, similar to the quark loops in the SM. Assuming that the interaction of the Higgs with the new particle i can be implemented by the substitution

$$m_i \to m_i\left(1 + g_{i,h}\frac{h}{v}\right) \tag{D1}$$

in its mass term, with $g_{i,h}$ an arbitrary $\mathcal{O}(1)$ constant, the effective coupling can be derived by means of low-energy theorems [4,15,16,66], which have been used in the calculation of various Higgs production and decay modes [4,67–70]. Similar approaches [52–57] are related to decoupling relations [71,72], which connect gauge couplings in the full theory to those in the effective theory with one or several degrees of freedom removed. The effective couplings can then be expressed [53] in terms of gauge independent objects like the $\overline{\text{MS}}$ β functions for the strong and electromagnetic coupling, and the QCD anomalous mass dimension γ_m of the heavy particle,[12]

$$c_{ggh} = -\frac{2\pi g_{i,h}}{\alpha_s^2(1-\gamma_m(\alpha_s'))}\left(\beta(\alpha_s) - \beta'(\alpha_s')\frac{\partial\alpha_s}{\partial\alpha_s'}\right), \tag{D2}$$

$$c_{\gamma\gamma h} = -\frac{2\pi g_{i,h}}{\alpha^2(1-\gamma_m(\alpha_s'))}\left(\beta_\gamma(\alpha,\alpha_s) - \beta_\gamma'(\alpha',\alpha_s')\frac{\partial\alpha}{\partial\alpha'} - \beta'(\alpha_s')\frac{\partial\alpha}{\partial\alpha_s'}\right). \tag{D3}$$

Quantities marked with a prime are to be evaluated in the full theory, i.e. including the heavy particle, while otherwise the effective theory without the heavy particle has to be employed. The pure QCD and mixed QED-QCD β functions are defined through

$$\beta(\alpha_s) \equiv \mu\frac{\mathrm{d}\alpha_s}{\mathrm{d}\mu} = -2\alpha_s\left[\epsilon + \left(\frac{\alpha_s}{4\pi}\right)\beta^0 + \left(\frac{\alpha_s}{4\pi}\right)^2\beta^1 + \mathcal{O}(\alpha_s^3)\right] \tag{D4}$$

and

$$\beta_\gamma(\alpha,\alpha_s) \equiv \mu\frac{\mathrm{d}\alpha}{\mathrm{d}\mu} = -2\alpha\left[\epsilon + \left(\frac{\alpha}{4\pi}\right)\beta_\gamma^0 + \left(\frac{\alpha}{4\pi}\right)\left(\frac{\alpha_s}{4\pi}\right)\beta_\gamma^1 + \mathcal{O}(\alpha^2,\alpha\alpha_s^2)\right], \tag{D5}$$

respectively. The anomalous mass dimension is given by

$$\gamma_m \equiv \frac{\mu}{m}\frac{\mathrm{d}m}{\mathrm{d}\mu} = -\left(\frac{\alpha_s}{4\pi}\right)\gamma_m^0 + \mathcal{O}(\alpha_s^2). \tag{D6}$$

Expanding the expressions (D2) and (D3) up to NLO in α_s we find

$$c_{ggh} = -g_{i,h}\left[\Delta\beta^0 + \left(\frac{\alpha_s}{4\pi}\right)(\Delta\beta^1 - \Delta\beta^0\gamma_m^0)\right] + \mathcal{O}(\alpha_s^2), \tag{D7}$$

$$c_{\gamma\gamma h} = -g_{i,h}\left[\Delta\beta_\gamma^0 + \left(\frac{\alpha_s}{4\pi}\right)(\Delta\beta_\gamma^1 - \Delta\beta_\gamma^0\gamma_m^0)\right] + \mathcal{O}(\alpha_s^2), \tag{D8}$$

where we defined

$$\Delta\beta^i = \beta'^i - \beta^i, \qquad \Delta\beta_\gamma^i = \beta_\gamma'^i - \beta_\gamma^i, \tag{D9}$$

i.e. the difference of the β-function coefficients in the full and effective theory.

1. Fermion

As a first example, we can consider a model with an additional heavy fermion F with electric charge Q_F in an arbitrary representation R of $SU(N_c)$:

$$\mathcal{L} = \mathcal{L}_{\text{SM}} + \bar{F}(i\not{D})F - m_F\left(1 + g_{F,h}\frac{h}{v}\right)\bar{F}F. \tag{D10}$$

We then find [73]

$$\Delta\beta^0 = -\frac{4}{3}T_R, \quad \Delta\beta^1 = -\left(\frac{20}{3}C_A + 4C_2(R)\right)T_R, \tag{D11}$$

$$\Delta\beta_\gamma^0 = -\frac{4}{3}d(R)Q_F^2, \quad \Delta\beta_\gamma^1 = -4C_2(R)d(R)Q_F^2, \tag{D12}$$

for the differences of β-function coefficients and

$$\gamma_m^0 = 6C_2(R), \tag{D13}$$

for the leading coefficient of the QCD anomalous mass dimension of the fermion, which is a known textbook result [74,75]. We checked (D13) by explicitly carrying out the mass renormalization of the fermion. Here $d(R)$, $C_2(R)$ and T_R are the dimension, the quadratic Casimir and the Dynkin index of representation R, respectively. The latter

[12] In the original references, decoupling relations were investigated with a heavy quark in mind, but the results can be used for scalar-induced Higgs-gluon and Higgs-photon interactions, too, assuming (D1) holds.

defines the normalization of the generators in the given group representation, $\mathrm{Tr}[T_R^a T_R^b] = T_R \delta^{ab}$. C_A is the quadratic Casimir of the adjoint representation. Plugging these quantities into (D7) and (D8) and omitting terms of $\mathcal{O}(\alpha_s^2)$, we obtain

$$c_{ggh} = \frac{4}{3} g_{F,h} T_R \left[1 + \left(\frac{\alpha_s}{4\pi}\right)(5C_A - 3C_2(R))\right], \quad \text{(D14)}$$

$$c_{\gamma\gamma h} = \frac{4}{3} g_{F,h} d(R) Q_F^2 \left[1 + \left(\frac{\alpha_s}{4\pi}\right)(-3C_2(R))\right]. \quad \text{(D15)}$$

For a fermion in the fundamental representation of $SU(N_c)$ with $N_c = 3$ we have

$$c_{ggh} = \frac{2}{3} g_{F,h} \left[1 + \frac{11}{4}\frac{\alpha_s}{\pi}\right], \quad \text{(D16)}$$

$$c_{\gamma\gamma h} = 4 g_{F,h} Q_F^2 \left[1 - \frac{\alpha_s}{\pi}\right]. \quad \text{(D17)}$$

Of course, this result coincides with the heavy-top limit in the SM.

2. Scalar

We can also consider[13] a scalar with electric charge Q_S in representation R of $SU(N_c)$,

$$\mathcal{L} = \mathcal{L}_{\mathrm{SM}} + |D_\mu S|^2 - m_S^2 S^* S \left[1 + \sum_n f_n \left(\frac{h}{v}\right)^n\right] - g_s^2 \lambda_S^{ijkl} S_i^* S_k^* S_j S_l, \quad \text{(D18)}$$

where $i, j, k, l = 1, \ldots, d(R)$ are color indices. The coupling constant for a single Higgs to the scalar according to (D1) is then given by[14]

$$g_{S,h} = \frac{f_1}{2}. \quad \text{(D19)}$$

In (D18) we assumed that the quartic coupling is proportional to g_s^2, as is the case in some supersymmetric scenarios. The coupling λ_S depends on the concrete model under consideration, but in any case obeys

$$(\lambda_S^{ijkl})^* = \lambda_S^{jilk}. \quad \text{(D20)}$$

Furthermore it is symmetric with respect to $i \leftrightarrow k$ and $j \leftrightarrow l$. If we are interested in a model where the four-scalar interaction does not contribute to the QCD corrections, and consequently does not affect the Higgs-gluon and Higgs-photon effective couplings to $\mathcal{O}(\alpha_s)$, we can simply set $\lambda_S = 0$ in the following results.

The β-function differences read [73]

$$\Delta\beta^0 = -\frac{1}{3} T_R, \quad \Delta\beta^1 = -\left(\frac{2}{3} C_A + 4C_2(R)\right) T_R, \quad \text{(D21)}$$

$$\Delta\beta_\gamma^0 = -\frac{1}{3} d(R) Q_S^2, \qquad \Delta\beta_\gamma^1 = -4C_2(R) d(R) Q_S^2. \quad \text{(D22)}$$

The scalar self-interaction does not enter the β functions before the three-loop level [77], but appears in the LO QCD anomalous mass dimension of the scalar,

$$\gamma_m^0 = 3C_2(R) - \frac{4}{d(R)} \sum_{i,k} \lambda_S^{iikk}. \quad \text{(D23)}$$

We derived γ_m^0 by explicit calculation of the mass renormalization of the scalar; our result agrees with [76]. Plugging everything into (D7) and (D8) we obtain [up to terms $\mathcal{O}(\alpha_s^2)$]

$$c_{ggh} = \frac{g_{S,h}}{3} T_R \left[1 + \left(\frac{\alpha_s}{4\pi}\right)\left(2C_A + 9C_2(R) + \frac{4}{d(R)} \sum_{i,k} \lambda_S^{iikk}\right)\right], \quad \text{(D24)}$$

$$c_{\gamma\gamma h} = \frac{g_{S,h}}{3} d(R) Q_S^2 \left[1 + \left(\frac{\alpha_s}{4\pi}\right)\left(9C_2(R) + \frac{4}{d(R)} \sum_{i,k} \lambda_S^{iikk}\right)\right]. \quad \text{(D25)}$$

For a scalar in the fundamental representation of $SU(N_c)$ with $N_c = 3$ we have

$$c_{ggh} = \frac{g_{S,h}}{6} \left[1 + \frac{9}{2}\frac{\alpha_s}{\pi}\right], \quad \text{(D26)}$$

$$c_{\gamma\gamma h} = g_{S,h} Q_S^2 \left[1 + 3\frac{\alpha_s}{\pi}\right], \quad \text{(D27)}$$

if the quartic interaction does not contribute. In case the scalar is a squark in the Minimal Supersymmetric Standard Model (MSSM), again in the fundamental representation, the coupling λ_S is given by [78,79]

$$\lambda_S^{ijkl} = \frac{1}{4}(T_{ij}^a T_{kl}^a + T_{il}^a T_{kj}^a) \Rightarrow \sum_{i,k} \lambda_S^{iikk} = \frac{1}{4} N_c C_F, \quad \text{(D28)}$$

[13] Only after we finished the following calculation we became aware of [76], in which a very similar model has been considered, focusing on the Higgs-gluon coupling.

[14] Note that upon integrating out the scalar, the Lagrangian (D18) also generates effective couplings involving an arbitrary number of Higgs particles. The derivation of the corresponding coupling constants requires a generalization of the expressions (D2) and (D3), which is beyond the scope of this Appendix. We will therefore restrict ourselves to the single Higgs case.

where T^a are the $SU(N_c)$ generators in the fundamental representation. For the effective couplings we then find ($N_c = 3$)

$$c_{ggh} = \frac{g_{S,h}}{6}\left[1 + \frac{29}{6}\frac{\alpha_s}{\pi}\right], \tag{D29}$$

$$c_{\gamma\gamma h} = g_{S,h}Q_S^2\left[1 + \frac{10}{3}\frac{\alpha_s}{\pi}\right]. \tag{D30}$$

Note that these results do not take any gluino exchange into account [80]. Our expressions agree with those presented in [8,70,76]. We again find consistent results by matching the scalar-loop induced amplitudes for $h \to \gamma\gamma$ [25] and $h \to gg$ [38] in the limit of infinite scalar mass to the amplitudes in the effective theory with local Higgs-photon and Higgs-gluon interactions.[15]

[15]Reference [25] does not include the quartic self-interactions into the calculation of $h \to \gamma\gamma$, while [38] presents the results for $h \to gg$ in the $m_S \to \infty$ limit both with and without it. For further details concerning the previous literature, see footnote 10 in [76].

[1] F. Feruglio, The chiral approach to the electroweak interactions, Int. J. Mod. Phys. A **08**, 4937 (1993).
[2] G. Buchalla, O. Catà, A. Celis, and C. Krause, Note on anomalous Higgs-boson couplings in effective field theory, Phys. Lett. B **750**, 298 (2015).
[3] U. Baur and E. W. Nigel Glover, Higgs boson production at large transverse momentum in hadronic collisions, Nucl. Phys. **B339**, 38 (1990).
[4] M. Spira *et al.*, Higgs boson production at the LHC, Nucl. Phys. **B453**, 17 (1995).
[5] W. Beenakker *et al.*, NLO QCD corrections to t anti-t H production in hadron collisions, Nucl. Phys. **B653**, 151 (2003).
[6] Vittorio Del Duca, Alberto Frizzo, and Fabio Maltoni, Higgs boson production in association with three jets, J. High Energy Phys. 05 (2004) 064.
[7] S. Borowka, N. Greiner, G. Heinrich, S. P. Jones, M. Kerner, J. Schlenk, and T. Zirke, Full top quark mass dependence in Higgs boson pair production at NLO, J. High Energy Phys. 10 (2016) 107.
[8] Michael Spira, Higgs boson production and decay at hadron colliders, Prog. Part. Nucl. Phys. **95**, 98 (2017).
[9] G. Buchalla, O. Catà, A. Celis, and C. Krause, Fitting Higgs data with nonlinear effective theory, Eur. Phys. J. C **76**, 233 (2016).
[10] G. Buchalla, M. Capozi, A. Celis, G. Heinrich, and L. Scyboz, Higgs boson pair production in non-linear effective field theory with full mt-dependence at NLO QCD, J. High Energy Phys. 09 (2018) 057.
[11] Gerhard Buchalla, Oscar Catà, and Claudius Krause, Complete electroweak chiral Lagrangian with a light Higgs at NLO, Nucl. Phys. **B880**, 552 (2014); **B913**, 475(E) (2016).
[12] Gerhard Buchalla, Oscar Catà, and Claudius Krause, On the power counting in effective field theories, Phys. Lett. B **731**, 80 (2014).
[13] Hao Sun, Ming-Lei Xiao, and Jiang-Hao Yu, Complete NLO operators in the Higgs effective field theory, arXiv: 2206.07722.
[14] Lukáš Gráf, Brian Henning, Xiaochuan Lu, Tom Melia, and Hitoshi Murayama, Hilbert series, the Higgs mechanism, and HEFT, J. High Energy Phys. 02 (2023) 064.
[15] John R. Ellis, Mary K. Gaillard, and Dimitri V. Nanopoulos, A phenomenological profile of the Higgs boson, Nucl. Phys. **B106**, 292 (1976).
[16] Mikhail A. Shifman *et al.*, Low-energy theorems for Higgs boson couplings to photons, Sov. J. Nucl. Phys. **30**, 711 (1979).
[17] Han- Qing Zheng and Dan- Di Wu, First order QCD corrections to the decay of the Higgs boson into two photons, Phys. Rev. D **42**, 3760 (1990).
[18] A. Djouadi, M. Spira, J.J. van der Bij, and P.M. Zerwas, QCD corrections to gamma gamma decays of Higgs particles in the intermediate mass range, Phys. Lett. B **257**, 187 (1991).
[19] S. Dawson and R. P. Kauffman, QCD corrections to $H \to \gamma\gamma$, Phys. Rev. D **47**, 1264 (1993).
[20] A. Djouadi, M. Spira, and P. M. Zerwas, Two photon decay widths of Higgs particles, Phys. Lett. B **311**, 255 (1993).
[21] K. Melnikov and Oleg I. Yakovlev, Higgs-two-photon interaction in the standard model. The QCD radiative correction, Phys. Lett. B **312**, 179 (1993).
[22] M. Inoue, R. Najima, T. Oka, and J. Saito, QCD corrections to two photon decay of the Higgs boson and its reverse process, Mod. Phys. Lett. A **09**, 1189 (1994).
[23] J. Fleischer, O. V. Tarasov, and V. O. Tarasov, Analytical result for the two loop QCD correction to the decay $H \to 2\gamma$, Phys. Lett. B **584**, 294 (2004).
[24] Robert Harlander and Philipp Kant, Higgs production and decay: Analytic results at next-to-leading order QCD, J. High Energy Phys. 12 (**2005**) 015.
[25] U. Aglietti, Roberto Bonciani, Giuseppe Degrassi, and Alessandro Vicini, Analytic results for virtual QCD corrections to Higgs production and decay, J. High Energy Phys. 01 (2007) 021.
[26] T. Kinoshita, Mass singularities of Feynman amplitudes, J. Math. Phys. (N.Y.) **3**, 650 (1962).
[27] T. D. Lee and M. Nauenberg, Degenerate systems and mass singularities, Phys. Rev. **133**, B1549 (1964).
[28] Roberto Contino, Margherita Ghezzi, Christophe Grojean, Margarete Mühlleitner, and Michael Spira, eHDECAY: An implementation of the Higgs effective Lagrangian into HDECAY, Comput. Phys. Commun. **185**, 3412 (2014).

[29] Roberto Contino, Margherita Ghezzi, Christophe Grojean, Margarete Mühlleitner, and Michael Spira, Effective Lagrangian for a light Higgs-like scalar, J. High Energy Phys. 07 (2013) 035.
[30] R. L. Workman *et al.*, Review of particle physics, Prog. Theor. Exp. Phys. **2022**, 083C01 (2022).
[31] Lance J. Dixon, E. W. Nigel Glover, and Valentin V. Khoze, MHV rules for Higgs plus multi-gluon amplitudes, J. High Energy Phys. 12 (2004) 015.
[32] S. D. Badger, E. W. Nigel Glover, and Valentin V. Khoze, MHV rules for Higgs plus multi-parton amplitudes, J. High Energy Phys. 03 (2005) 023.
[33] A. Gehrmann-De Ridder, T. Gehrmann, and E. W. Nigel Glover, Antenna subtraction at NNLO, J. High Energy Phys. 09 (2005) 056.
[34] A. Daleo, T. Gehrmann, and D. Maitre, Antenna subtraction with hadronic initial states, J. High Energy Phys. 04 (2007) 016.
[35] James Currie, E. W. N. Glover, and Steven Wells, Infrared structure at NNLO using antenna subtraction, J. High Energy Phys. 04 (2013) 066.
[36] Carola F. Berger, Vittorio Del Duca, and Lance J. Dixon, Recursive construction of Higgs-plus-multiparton loop amplitudes: The last of the Phi-nite loop amplitudes, Phys. Rev. D **74**, 094021 (2006); **76**, 099901(E) (2007).
[37] Stefano Catani, The singular behavior of QCD amplitudes at two loop order, Phys. Lett. B **427**, 161 (1998).
[38] Charalampos Anastasiou, Stefan Beerli, Stefan Bucherer, Alejandro Daleo, and Zoltan Kunszt, Two-loop amplitudes and master integrals for the production of a Higgs boson via a massive quark and a scalar-quark loop, J. High Energy Phys. 01 (2007) 082.
[39] J. S. Rozowsky, Feynman diagrams and cutting rules, arXiv: hep-ph/9709423.
[40] P. De Causmaecker *et al.*, Multiple bremsstrahlung in gauge theories at high-energies. 1. General formalism for quantum electrodynamics, Nucl. Phys. **B206**, 53 (1982).
[41] R. Kleiss and W. James Stirling, Spinor techniques for calculating $pp \to W^{\pm}/Z^0 +$ Jets, Nucl. Phys. **B262**, 235 (1985).
[42] Zhan Xu, Da-Hua Zhang, and Lee Chang, Helicity amplitudes for multiple bremsstrahlung in massless non-Abelian gauge theories, Nucl. Phys. **B291**, 392 (1987).
[43] Lance J. Dixon, A brief introduction to modern amplitude methods, *Theoretical Advanced Study Institute in Elementary Particle Physics: Particle Physics: The Higgs Boson and Beyond* (2014), pp. 31–67, 10.5170/CERN-2014-008.31.
[44] Henriette Elvang and Yu-tin Huang, Scattering amplitudes, arXiv:1308.1697.
[45] R. Keith Ellis *et al.*, Higgs decay to $\tau^+\tau^-$: A possible signature of intermediate mass Higgs bosons at the SSC, Nucl. Phys. **B297**, 221 (1988).
[46] T. Hahn, CUBA: A library for multidimensional numerical integration, Comput. Phys. Commun. **168**, 78 (2005).
[47] K. G. Chetyrkin, Johann H. Kühn, and M. Steinhauser, RunDec: A *Mathematica* package for running and decoupling of the strong coupling and quark masses, Comput. Phys. Commun. **133**, 43 (2000).
[48] Barbara Schmidt and Matthias Steinhauser, CRunDec: A C++ package for running and decoupling of the strong coupling and quark masses, Comput. Phys. Commun. **183**, 1845 (2012).
[49] Florian Herren and Matthias Steinhauser, Version 3 of RunDec and CRunDec, Comput. Phys. Commun. **224**, 333 (2018).
[50] Federico Buccioni, Jean-Nicolas Lang, Jonas M. Lindert, Philipp Maierhöfer, Stefano Pozzorini, Hantian Zhang, and Max F. Zoller, OpenLoops 2, Eur. Phys. J. C **79**, 866 (2019).
[51] A. Gehrmann-De Ridder, T. Gehrmann, and E. W. Nigel Glover, Gluon-gluon antenna functions from Higgs boson decay, Phys. Lett. B **612**, 49 (2005).
[52] Michael Kramer, Eric Laenen, and Michael Spira, Soft gluon radiation in Higgs boson production at the LHC, Nucl. Phys. **B511**, 523 (1998).
[53] K. G. Chetyrkin, Bernd A. Kniehl, and M. Steinhauser, Decoupling relations to $O(\alpha_s^3)$ and their connection to low-energy theorems, Nucl. Phys. **B510**, 61 (1998).
[54] Y. Schröder and M. Steinhauser, Four-loop decoupling relations for the strong coupling, J. High Energy Phys. 01 (2006) 051.
[55] K. G. Chetyrkin, Johann H. Kühn, and Christian Sturm, QCD decoupling at four loops, Nucl. Phys. **B744**, 121 (2006).
[56] P. A. Baikov and K. G. Chetyrkin, Top Quark Mediated Higgs Boson Decay into Hadrons to Order α_s^5, Phys. Rev. Lett. **97**, 061803 (2006).
[57] Michael Spira, Effective multi-Higgs couplings to gluons, J. High Energy Phys. 10 (**2016**) 026.
[58] Jorge de Blas, Otto Eberhardt, and Claudius Krause, Current and future constraints on Higgs couplings in the nonlinear effective theory, J. High Energy Phys. 07 (2018) 048.
[59] B. Grzadkowski, M. Iskrzyński, M. Misiak, and J. Rosiek, Dimension-six terms in the standard model Lagrangian, J. High Energy Phys. 10 (**2010**) 085.
[60] G. Buchalla *et al.*, Loop counting matters in SMEFT, arXiv:2204.11808.
[61] A. Dedes, W. Materkowska, M. Paraskevas, J. Rosiek, and K. Suxho, Feynman rules for the standard model effective field theory in R_ξ-gauges, J. High Energy Phys. 06 (2017) 143.
[62] Gudrun Heinrich, Jannis Lang, and Ludovic Scyboz, SMEFT predictions for $gg \to hh$ at full NLO QCD and truncation uncertainties, J. High Energy Phys. 08 (2022) 079.
[63] Andreas Helset, Adam Martin, and Michael Trott, The geometric standard model effective field theory, J. High Energy Phys. 03 (2020) 163.
[64] Tyler Corbett, Adam Martin, and Michael Trott, Consistent higher order $\sigma(\mathcal{GG} \to h)$, $\Gamma(h \to \mathcal{GG})$ and $\Gamma(h \to \gamma\gamma)$ in geoSMEFT, J. High Energy Phys. 12 (2021) 147.
[65] Adam Martin and Michael Trott, *ggh* variations, Phys. Rev. D **105**, 076004 (2022).
[66] Bernd A. Kniehl and Michael Spira, Low-energy theorems in Higgs physics, Z. Phys. C **69**, 77 (1995).
[67] Bernd A. Kniehl and Michael Spira, Two loop $O(\alpha_s G_F m_t^2)$ correction to the $H \to b\bar{b}$ decay rate, Nucl. Phys. **B432**, 39 (1994).

[68] Bernd A. Kniehl and Michael Spira, Two loop $O(\alpha_s G_F m_t^2)$ corrections to Higgs production at LEP, Nucl. Phys. **B443**, 37 (1995).

[69] S. Dawson, A. Djouadi, and M. Spira, QCD Corrections to SUSY Higgs Production: The Role of Squark Loops, Phys. Rev. Lett. **77**, 16 (1996).

[70] Margarete Mühlleitner and Michael Spira, Higgs boson production via gluon fusion: Squark loops at NLO QCD, Nucl. Phys. **B790**, 1 (2008).

[71] Werner Bernreuther and Werner Wetzel, Decoupling of heavy quarks in the minimal subtraction scheme, Nucl. Phys. **B197**, 228 (1982); **B513**, 758(E) (1998).

[72] S. A. Larin, T. van Ritbergen, and J. A. M. Vermaseren, The large quark mass expansion of $\Gamma(Z^0 \to \text{hadrons})$ and $\Gamma(\tau^- \to \nu_\tau + \text{hadrons})$ in the order $\alpha_s{}^3$, Nucl. Phys. **B438**, 278 (1995).

[73] D. R. T. Jones, The two loop beta function for a $G(1) \times G(2)$ gauge theory, Phys. Rev. D **25**, 581 (1982).

[74] Michael E. Peskin and Daniel V. Schroeder, *An Introduction to Quantum Field Theory* (Addison-Wesley, Reading, MA, 1995), ISBN: 978-0-201-50397-5.

[75] Matthew D. Schwartz, *Quantum Field Theory and the Standard Model* (Cambridge University Press, Cambridge, England, 2014), ISBN: 978-1-107-03473-0.

[76] Stefania Gori and Ian Low, Precision Higgs measurements: Constraints from new oblique corrections, J. High Energy Phys. 09 (2013) 151.

[77] Thomas Curtright, Three-loop charge renormalization effects due to quartic scalar self-interactions, Phys. Rev. D **21**, 1543 (1980).

[78] Adel Bilal, Introduction to supersymmetry, arXiv:hep-th/0101055.

[79] M. Shifman, *Advanced Topics in Quantum Field Theory: A Lecture Course* (Cambridge University Press, Cambridge, England, 2012), ISBN: 978-1-139-21036-2, 978-0-521-19084-8.

[80] Margarete Mühlleitner, Heidi Rzehak, and Michael Spira, MSSM Higgs boson production via gluon fusion: The large gluino mass limit, J. High Energy Phys. 04 (2009) 023.